NTNU

Norwegian University of
Science and Technology

The Effect of Fiber Reinforcement on Crack Development due to Restraint of Concrete Structures

Elisabeth Leite Skare

Civil and Environmental Engineering
Submission date: June 2016
Supervisor: Terje Kanstad, KT
Co-supervisor: Kathrin Sandstad, Statens vegvesen
Håvard Johansen, Statens vegvesen

Norwegian University of Science and Technology
Department of Structural Engineering

Department of Structural Engineering
Faculty of Engineering Science and Technology
NTNU- Norwegian University of Science and Technology

ACCESSIBILITY

OPEN

MASTER THESIS 2016

SUBJECT AREA:	DATE:	NO. OF PAGES:
Concrete Technology	09.06.16	16 + 82 +10

TITLE:

The Effect of Fiber Reinforcement on Crack Development due to Restraint of Concrete Structures

BY:

Elisabeth Leite Skare

SUMMARY:
This thesis studies the effect of fiber reinforcement on crack development in concrete structures. Background for choice of subject, is that cracks due to external restraint are observed on many of today's bridges, and it is assumed that fiber reinforcement may limit this crack development. Hence, a laboratory experiment was performed during the summer of 2015, in connection with the specialization project written by the undersigned. The experiment studied the effect of steel fibers and polymer fibers on the crack development, compared to a concrete without fiber reinforcement. In the fiber mixes, one saw a much denser crack development than for the reference concrete, and the crack widths were much smaller in the fiber mixes.

On the initiative of Norwegian Public Roads Administration, it was decided to carry out the same measures to reduce cracks on a real bridge. This full-scale experiment has been conducted in connection with this thesis. The chosen bridge is the pedestrian and bicycle bridge Sandsgård Bridge in Ganddal, close to Sandnes. The bridge is 50 meters long and the edge beams, á 16 meters, were cast with six different concrete mixes, five of them containing fiber reinforcement.

First some relevant theoretical background is presented, and three models for calculation crack widths are introduced. Then a brief description of the laboratory experiment is presented, followed by a description of the full-scale experiment on Sandsgård Bridge. Calculations of the crack widths are performed for the two experiments.

Simulations of the two experiments are performed in the finite element program, CrackTeStCOIN. This computer program is used for simulation of the temperature and stress development of the experiments. Based on the simulated stresses, and an assumption of an effective elastic modulus of 10 000 MPa and 12 000 MPa for the laboratory and full-scale experiment respectively, the occurring strains are calculated. The simulated strains are compared with the strains obtained from the three investigated calculation models.

Lastly, the effect of the different fiber reinforcement are discussed.

RESPONSIBLE TEACHER: Professor Terje Kanstad

SUPERVISOR: Professor Terje Kanstad

CARRIED OUT AT: The Department of Structural Engineering, NTNU

Institutt for konstruksjonsteknikk
Fakultet for ingeniørvitenskap og teknologi
NTNU- Norges teknisk- naturvitenskapelige universitet

TILGJENGELIGHET

ÅPEN

MASTEROPPGAVE 2016

FAGOMRÅDE:	DATO:	ANTALL SIDER:
Betongteknologi	09.06.16	16 + 82 + 10

TITTEL:

Virkning av fiberarmering på fastholdningsriss i betongkonstruksjoner

UTFØRT AV:

Elisabeth Leite Skare

SAMMENDRAG:
Denne oppgaven tar for seg virkningen av fiberarmering på rissutvikling i betongkonstruksjoner. Bakgrunn for oppgavens tema, er at det er observert fastholdningsriss på kantdragerne på mange av dagens broer. Det antas at fiberarmering kan begrense slik rissutvikling, og det ble derfor utført et laboratorieforsøk, sommeren 2015, i forbindelse med fordypningsprosjektet til undertegnede. Forsøket studerte effekten av stålfiber og polymerfiber på rissutvikling, sammenlignet med rissutviklingen i en betongbjelke uten fiberarmering. I fiberbetongene ble det observert en mye tettere rissopptreden enn i referansebetongen, og for fiberbetongene var rissviddene mindre enn for referansebetongen.

Etter initiativ fra Statens Vegvesen ble det bestemt å utføre de samme rissreduserende tiltakene på en ekte bro. Dette fullskala-forsøket er blitt utført i forbindelse med denne oppgaven. Den valgte broen er gang- og sykkelbroen Sandsgård Bro i Ganddal, i nærheten av Sandnes. Broen er 50 meter lang, og kantdragerne á 16 meter, ble støpt med seks ulike betongblandinger, hvor av fem inneholdt fiberarmering.

Først blir relevant bakgrunnsteori presentert, og tre beregningsmodeller for rissvidder blir introdusert. Deretter blir en kort beskrivelse av laboratorieforsøket gitt, etterfulgt av en beskrivelse av fullskala-forsøket på Sandsgård Bro. Rissvidde-beregninger etter beregningsmodellene er utført for begge forsøkene.

Simuleringer av de to forsøkene er utført i elementprogrammet CrackTeStCOIN. Dette dataprogrammet blir brukt til å estimere temperatur- og spenningsutviklingen til de to forsøkene. Basert på de simulerte spenningene, og en antagelse om en effektiv E-modul lik henholdsvis 10 000 MPa og 12 000 MPa for laboratorie- og fullskalaforsøket, beregnes de opptredende tøyningene. Disse blir sammenlignet med de beregnede tøyningene fra beregningsmodellene.

Til slutt blir effekten av de ulike fiberarmeringene drøftet.

FAGLÆRER: Professor Terje Kanstad

VEILEDER: Professor Terje Kanstad

UTFØRT VED: Institutt for konstruksjonsteknikk, NTNU

Preface

This Masters thesis was written at the Department of Structural Engineering at the Norwegian University of Science and Technology in Trondheim, during the autumn 2016. The thesis is a requirement for the degree of Master of Science, and finalized my study in the programme Civil and Environmental Engineering, with specialization in Structural Engineering.

First, I would like to thank Researcher Giedrius Zirgulis at NTNU for conducting the residual flexural bending strength tests, as well as providing assistance with the experimental set up. I will also like to thank Engineer Steinar Seehuus, Staff Engineer Ove Loraas and Staff Engineer Gøran Loraas for good guidance at the laboratory and for providing the required equipment, both in conjunction with this thesis and the specialization project.

A special thanks is given to Nils Bergfinn Haaland at Skanska, for your warm welcome at Sandsgård Bridge, and for providing required equipment at the construction site, as well as useful information by mail. Also, Stian Persson, Kathrin Sandstad and Sascha Baarck at the Norwegian Public Roads Administration, have been helpful with providing the necessary drawings and information by mail, and supervision on the construction site. Concrete technologist Arne Vatnar at Skanska Teknikk has been helpful with providing material information by mail. He has installed the heating cables at Sandsgård Bridge, and processed the temperature data in excel. He also has participated in casting of the edge beams, and the prisms for testing of the residual flexural tensile strength.

I would also like thank Anja Birgitta Estenstad Klausen for help regarding the finite element program CrackTeStCOIN.

Finally, I would like to thank my main supervisor, Professor Terje Kanstad; first of all for good guidance, supervision and feedback. He has shown great interest in the topic, as evidenced by the fact that he travelled to Sandnes with me on a construction site visit. Secondly, I would like to thank him for contributing with relevant background theory and his eager for follow-up meetings. He has been willingly answering my questions and helping with the proofreading.

Trondheim, June 9, 2016

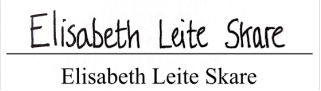

Elisabeth Leite Skare

Abstract

This thesis studies the effect of fiber reinforcement on crack development in concrete structures. Background for choice of subject, is that cracks due to external restraint are observed on many of today's bridges, and it is assumed that fiber reinforcement may limit this crack development. Hence, a laboratory experiment was performed during the summer of 2015, in connection with the specialization project written by the undersigned. The experiment studied the effect of steel fibers and polymer fibers on the crack development, compared to a concrete without fiber reinforcement. In the fiber mixes, one saw a much denser crack development than for the reference concrete, and the crack widths were much smaller in the fiber mixes.

On the initiative of Norwegian Public Roads Administration, it was decided to carry out the same measures to reduce cracks on a real bridge. This full-scale experiment has been conducted in connection with this thesis. The chosen bridge is the pedestrian and bicycle bridge Sandsgård Bridge in Ganddal, close to Sandnes. The bridge is 50 meters long and the edge beams, à 16 meters, were cast with six different concrete mixes, five of them containing fiber reinforcement.

First some relevant theoretical background is presented, and three models for calculation crack widths are introduced. Then a brief description of the laboratory experiment is presented, followed by a description of the full-scale experiment on Sandsgård Bridge. Calculations of the crack widths are performed for the two experiments.

Simulations of the two experiments are performed in the finite element program, CrackTeSt-COIN. This computer program is used for simulation of the temperature and stress development of the experiments. Based on the simulated stresses, and an assumption of an effective elastic modulus of 10 000 MPa and 12 000 MPa for the laboratory and full-scale experiment respectively, the occurring strains are calculated. The simulated strains are compared with the strains obtained from the three investigated calculation models.

Lastly, the effect of the different fiber reinforcement are discussed.

Contents

Nomenclature

α_e, η	The modular ratio E_s/E_{cm}
α_T	The coefficient of thermal expansion in concrete
ΔT	Temperature difference
$\Delta\sigma_{ca}$	Concrete stress due to autogenous shrinkage
$\Delta\varepsilon_T$	The thermal dilation
ϕ,ϕ_b	The reinforcement bar diameter
ϕ^*	The final creep coefficient
ϕ_{ef}	The effective creep coefficient
ρ	The ratio A_s/A_{ct}
σ_T	Concrete stress due to tempeature changes
σ_{av}	The average concrete stress
σ_{c1}	Compressive stress in concrete
σ_{s1}	Compressive stress in reinforcement
σ_{s2}	Tensile stress in reinforcement
σ_s	The stress in the reinforcement
$\varepsilon_{ca}(t)$	The autogenous shrinkage strain in concrete
ε_{cr}	The crack-inducing strain
ε_{ctu}	The tensile strain capacity
ε_{free}	The strain which would occur if the member was completely unrestrained
ε_r	Restrained strain
A_I	$A_c + A_s(\frac{E_s}{E_c} - 1)$

A_n The cross-sectional area of the new (restrained) pour

A_o The cross-sectional area of the old (restraining) concrete

A_s The reinforcement area

A_{ct} The area of concrete in tension

A_{ef} The effective concrete area equal to $b \times h_{ef}$, where h_{ef} is the part of the tensile zone which has the same centre of gravity as the reinforcement

$A_{s,min}$ The minimum area of reinforcement

E_c The modulus of elasticity of the concrete

E_n The modulus of elasticity of the new pour concrete

E_o The modulus of elasticity of the old concrete

E_s The modulus of elasticity of the reinforcement

f_t The tensile strength of the concrete

$f_{ckt,0.05}$ 70% of the mean axial tensile strength of the concrete

f_{ck} The compressive strength of the concrete

f_{cm} The average compressive concrete strength

$f_{ct,eff}$ The mean value of the tensile strength of the concrete effective at the time when the cracks may first be expected to occur

f_{ctm} The average tensile strength of the concrete

f_{fres} The residual flexural tensile strength

f_{R1} The characteristic residual flexural tensile strength at a crack mouth opening displacement of 0.5 mm

f_{yk} Characteristic yield strength of the reinforcement

k The coefficient which allows for the effect of non-uniform self-equilibrating stresses, which lead to a reduction of restraint forces

k_c A coefficient which takes account of the stress distribution within the section immediately prior to cracking and of the change of the lever arm

l The length of the member

n,m The number of cracks

$N(\sigma_s, f_{ft,res})$ The force acting on un-cracked parts of the concrete

N_1 The force required to initiate a new crack

N_{cr} The restraining force in concrete

R The degree of restraint, where $R = 0$ for no restraint and $R = 1$ for full restraint

R_1 The restraint factor that applies during the early thermal cycle

R_2 The restraint factor applying to medium and long-term deformation

R_3 The restraint factor applying to drying shrinkage

R_j The restraint at the joint

R_{ax} A factor defining the degree of external restraint provided by elements attached to the element considered

R_{edge} The edge restraint factor at the location of the maximum crack width

s_0 The distance over which the concrete and steel stresses vary

$s_{r,max}$ The maximum crack spacing

t The age of the concrete at the given time

T_1 The difference between the peak temperature and the mean ambient temperature at the end of the thermal cycle

T_2 The difference between the mean ambient temperature at the end of the early thermal cycle and the minimum element temperature likely in the course of the element life

t_s The age of the concrete in days at the beginning of drying.

w/c The water/cement-ratio in concrete.

w_k, w The crack width

$(\varepsilon_{sm} - \varepsilon_{cm})$ The difference in deformation between the steel and the concrete over the maximum crack spacing

α_c The coefficient of thermal expansion in concrete

ϵ_1^* The final concrete strain

ϵ_c^* The final creep strain

ϵ_e The final elastic strain

ϵ_{s1}^* The final steel strain

ϵ_{sh}^* The final shrinkage strain

ε_c Creep strain in concrete

ε_{sh} Shrinkage strain in concrete

E_{eff} Effective modulus of elasticity of concrete

Chapter 1

Introduction

1.1 Background

This master thesis is written as a continuation of the specialization project written by the undersigned. On many of today's bridges, the edge beams are cast some weeks after the casting of the bridge deck. Temperature differences between two subsequent casting operations give a disadvantageous stress development in the concrete structure. The most commonly used structure to illustrate this is the wall cast on an existing foundation. During heating the newly cast structure, the wall, expands freely, due to its low stiffness. In the cooling phase, however, the wall has developed considerable strength and stiffness, at the same time as the adhesion against the foundation is almost fully developed. The foundation will restrain the contraction in the wall during the cooling. This external restraint will induce tensile stresses in the wall, which in turn may cause cracks, as shown in Figure 1.1. [1]

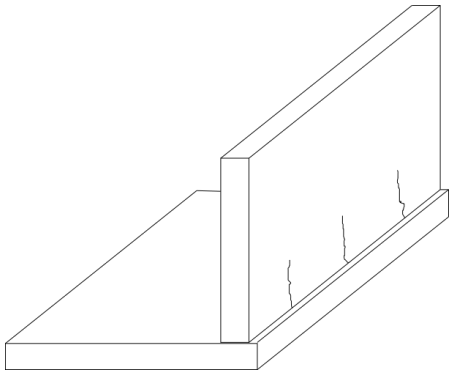

FIGURE 1.1: Crack development due to external restraint. Image adapted from *Concrete Technology 1, TKT 4215* [1].

Such cracks do often go through the entire thickness of the structure, and may reduce the quality of the structure. For instance, does the high alkalinity of the concrete's pore solution lead to a formation of a thin, dense film of corrosion products on the reinforcement bar surface. Cracks may lead chloride ions or carbon dioxide gas in to the steel, which will lower the pH in the

concrete. This may destroy the thin protective layer, which in turn may lead to corrosion, as shown in Figure 1.2. This may lead to a reduced cross section of the reinforcement, further cracking of the concrete or hydrogen embrittlement. [1]

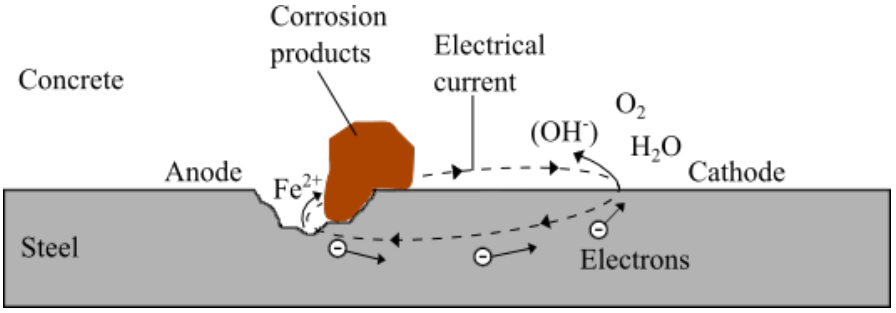

FIGURE 1.2: The electrochemical reactions in the corrosion process. Image adapted from *Concrete Technology 1, TKT 4215* [1].

Due to the fact that many structural elements in bridges are exposed to external restraint, a laboratory experiment was carried out in connection with the specialization project, intentionally to reduce cracks in edge beams by the use of fiber reinforcement. The experiment studied the effect of steel fibers and polymer fibers on the crack development, compared to a concrete without fiber reinforcement.

The experiment showed that the fiber reinforcement had a very positive effect on the crack development. In the fiber mixes, one saw a much denser crack development than for the reference concrete, and the crack widths were much smaller in the fiber mixes. The steel fibers reduced the average crack width by a factor of 4-5, while the polymer fibers reduced the crack width by a factor of 2-3. This effect is favorable for the concrete, since it reduces the risk of corrosion, and improves the aesthetics of the concrete surface.

A model for calculating crack widths, developed by Ingemar Löfgren [2], was used to calculate the expected crack widths in the edge beams. The measured crack widths were compared with the calculated values, shown in Table 1.1. The calculation model is only valid for a member that is fully restrained in both ends, which may explain parts of the differences in the calculated and measured values. In this master thesis the model is studied, and due to the scope of the thesis, the model has been modified to account for the considered edge beams.

TABLE 1.1: Average measured crack widths and calculated maximum crack widths for the edge beams in the laboratory experiment.

Concrete mix	Measured crack width (average)	Calculated crack width (maximum)
Reference mix	0.17	0.09
Concrete with steel fibers	0.03-0.04	0.02
Concrete with polymer fibers	0,06	0.03

Two other calculation models for crack widths are also presented and used in this thesis. These are not taking the effect of fiber reinforcement into account in the calculation, and are therefore only performed on the reference beams.

On the initiative of Norwegian Public Roads Administration, Region West, it was decided to carry out the same measures as in the laboratory experiment, to reduce cracks on a real bridge. This large-scale experiment has been conducted in connection with this thesis. The chosen bridge is the pedestrian and bicycle bridge Sandsgård Bridge in Ganddal, close to Sandnes. The bridge is 50 meters long and the edge beams were cast with six different concrete mixes, five of them containing fiber reinforcement. Two of the presented calculation models are used to calculate the theoretical crack widths on this bridge.

CrackTeStCOIN is a finite element computer program, that simulates temperatures and stresses in concrete. This program is used to estimate the stress case for both the laboratory experiment and the full-scale experiment. The concrete strain are derived from the estimated stresses, and the modeled and calculated strains are later compared.

Chapter 2

Theory

This chapter includes some relevant theoretical background. First the temperature effects on concrete is discussed, followed by creep and shrinkage in concrete. Then, strains and stresses in concrete subjected to restrained imposed deformations are discussed. Further, measures to reduce effects of cracking is presented. Lastly, a procedure for early-age thermal crack control is presented.

2.1 General

Concrete has a low tensile strength and tensile strain capacity, and the crack development starts already at a tensile strain of about 0.1 ‰. The drying shrinkage of concrete is about 0.6-0.8 ‰, which means that it is almost impossible to avoid cracking. Hence, reinforcement is needed to control the behaviour after cracking and to limit the crack widths. Large crack widths may lead to accelerated reinforcement corrosion in severe environments, leakage in water-retaining/resisting structures, insanitary conditions, or obstructions and interruptions in production processes. [2]

By preventing cracking, the chance that water can lead harmful salts into the reinforcement decreases, and thus decreases the risk of corrosion of the reinforcement. With knowledge of how and why cracks occurs, it is possible to select a concrete composition and execution that ensures durability [3].

2.2 Temperature

The temperature changes that occurs during the hardening phase and due to climate variations, lead to deformation of the concrete. This deformation is called thermal dilation, and is expressed by the equation:

$$\Delta\varepsilon_T = \Delta T \times \alpha_T \tag{2.1}$$

where $\Delta\varepsilon_T$ is the thermal dilation, ΔT is the temperature difference and α_T is the coefficient of thermal expansion.

In a restraint case may such temperature loads lead to thermal cracking. The thermal effect is generally the main contributor to stresses in concrete in the hardening phase [1]. In the Norwegian Public Roads Administration's *Prosesskode 2* the following temperature requirements, illustrated in Figure 2.1, have been formulated to limit the amount of early age cracking:

- The maximum temperature shall at no time exceed 65 °C.
- The temperature differential over the cross-section shall not exceed 20 °C
- The difference between the average temperatures in two adjacent cast sections shall not exceed 15 °C if the restraining length between cast sections exceeds 5 metres.

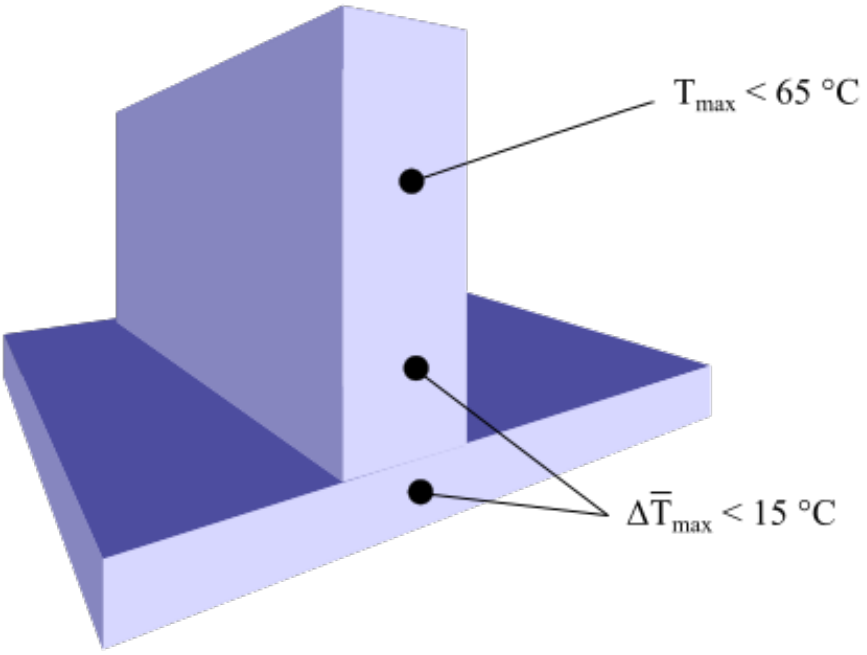

FIGURE 2.1: Temperature requirements in accordance with the Norwegian Public Roads Administration. Figure adapted from Concrete Technology 1 TKT 4215 [1].

2.3 Effect of Temperature on the Material Properties of Concrete

2.3.1 General

This section covers the temperature effects on the material properties strength, stiffness and creep of temperatures in the range -25°C to 200°C. All literature presented in this section is obtained from Eurocode 2: Design of concrete structures, Part 3: Liquid retaining and containment structures - Annex K [4]. While reading, it is important to keep in mind that the changes are strongly dependent on the particular type of concrete used.

2.3.2 Material Properties at Sub-zero Temperatures

When concrete is cooled below zero, its strength and stiffness increases. The higher the moisture content is, the greater the increase in strength and stiffness is. For saturated concrete, a cooling of the concrete to -25°C leads to an increase of around 30 MPa in compressive strength, while the same cooling leads to an increase of around 5 MPa for partially dry concrete. Cooling concrete to - 25°C leads to an increase in the modulus of elasticity of around 8000 MPa for saturated concrete and 2000 MPa for partially dry concrete.

2.3.3 Material Properties at Elevated Temperatures

Youngs modulus may be assumed to be unaffected by temperature up to 50°C. For higher temperatures, a linear reduction may be assumed up to a reduction of 20 % at a temperature of 200 °C.

The creep coefficient may be assumed to increase with increasing temperature above 20°C for concrete heated prior to loading. Table 2.1 presents the appropriate creep coefficient multipliers.

Table 2.1: Creep coefficient multiplier for different temperatures.

Temperature (°C)	Creep coefficient multiplier
20	1.00
50	1.35
100	1.96
150	2.58
200	3.20

If the load is present during heating of the concrete, this will lead to excess deformations that are irrecoverable.

2.4 Creep and Shrinkage of Concrete

Normally there will exist quite large stresses between the constituents in concrete, due to the inhomogeneous structure. This stress case arises partly because of the differences in the elastic and thermal properties between the cement paste and the aggregates. Another important reason is the tendency to volume reduction in the cement paste during drying.

When concrete is exposed to external forces, the internal and external forces will superimpose. This leads to a stress case where the elements are partly less or larger than in the stress case for the external stresses. Creep is time dependent deformation in a material, due to external loading [5]. Shrinkage is change in volume, due to change in the concretes moisture content [6].

If inconsistent drying is the case, the cement paste will be in tension and the coarse aggregates in compression. A stress case like this may explain the many conditions which occur during deformation of concrete [7].

A study of the specific effect of periodic variation in stresses, showed that a characteristic stress applied as a constant stress equalised the varying stresses within the reasonable limits, so far as the development of creep was concerned. Periodic changes in moisture conditions during the first months of loading influenced the creep, as well as the shrinkage. It was found that immersion in water for short periods of time also reduces the long-time values of creep and shrinkage [7].

2.5 Autogenous Shrinkage

The autogenous shrinkage is the self-produced shrinkage of the concrete. When cement and water reacts, the reaction product fills a smaller volume than the reactants, and chemical shrinkage occurs. At full hydration for a cement paste with w/c = 0.40, a volume loss of approximately 8 % is estimated. This volume loss creates chemical shrinkage pores. During further hydration these pores are partly emptied, which leads to a decrease in relative humidity within the concrete. This phenomena is called self-desiccation. The process creates capillary forces and under-pressure in the pore water. This results in an external contraction of the concrete, which is called autogenous shrinkage. For high strength concrete it is not unusual that the autogenous shrinkage is 0.1 - 0.2 ‰, while the tensile strain capacity of concrete generally is around 0.1 ‰. Naturally this will give rise to problems in practice. [1]

Most of the autogenous shrinkage strain develops in the early age of the concrete. According to Eurocode 2, Part 1-1, 3.1.4 (6) the autogenous shrinkage strain is given by the equation:

$$\varepsilon_{ca}(t) = \beta_{as}(t)\varepsilon_{ca}(\infty) = (1 - \mathrm{e}^{-0.2t^{0.5}}) \times 2.5(f_{ck} - 10) \times 10^{-6} \tag{2.2}$$

[8]

2.6 Strains and Stresses in Concrete Sections Subjected to Restrained Imposed Deformations

All literature presented in this section is obtained from Eurocode 2: Design of concrete structures, Part 3: Liquid retaining and containment structures - Annex L [4].

The strain in an uncracked concrete section is calculated from factors defining the degree of both axial and moment restraint. These factors are dependent on the stiffness of the element considered, and the geometry of the members attached to it. Restraint factors for a wall on a base is shown in Figure 2.2, and Table 2.2 presents the restraint factors for a central zone in a wall.

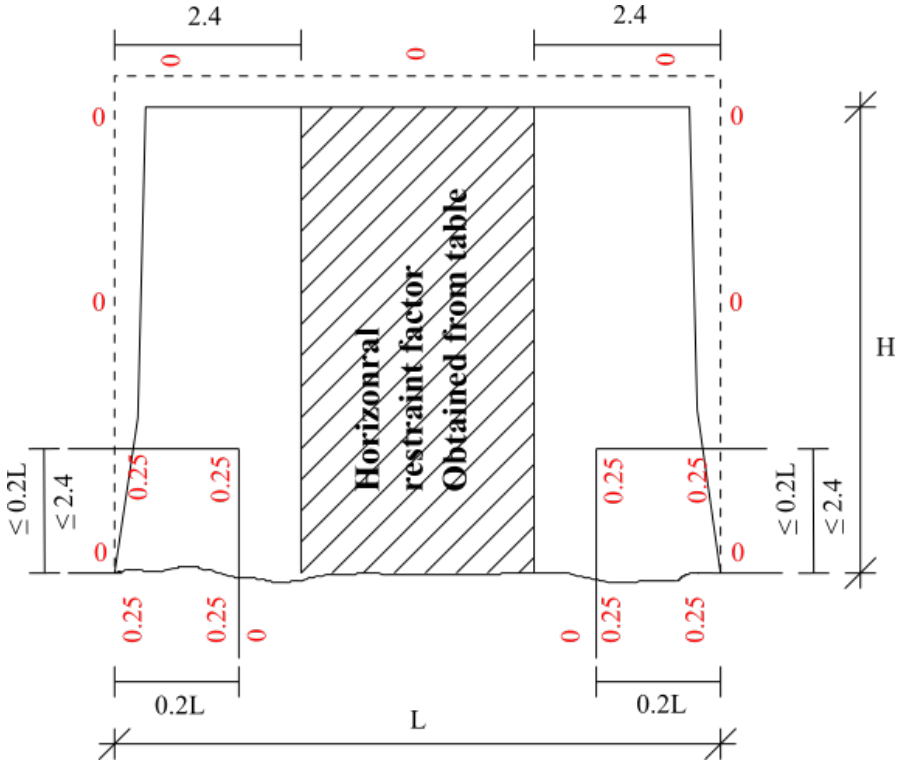

FIGURE 2.2: Restraint factors for wall on base. Figure adapted from Eurocode 2, Part 3, Annex L [4].

TABLE 2.2: Restraint factors in central zone.

Ratio L/H	Restraint factor at base	Restraint factor at top
1	0.5	0
2	0.5	0
3	0.5	0.05
4	0.5	0.3
>8	0.5	0.5

The stresses in concrete are calculated from the strains, and are consequently also dependent of the restraint.

2.7 Calculation of Crack Widths due to Restraint of Imposed Deformations

All literature presented in this section is obtained from Eurocode 2: Design of concrete structures, Part 3: Liquid retaining and containment structures - Annex M [4].

2.7.1 General

This section covers shrinkage and the early thermal movement due to cooling of members right after casting. Two practical problems, related to different forms of restraint, are investigated. The restraint along a members ends and restraint along one edge are studied, illustrated in Figure 11.1. The first-mentioned occurs when a new section of concrete is cast between two pre-existing sections, while the second case arises where a wall is cast onto a pre-existing stiff base.

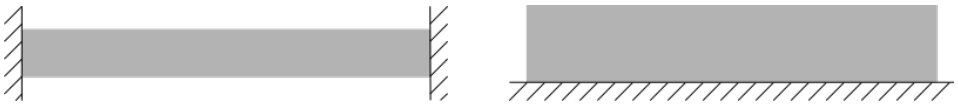

(a) Restraint of a member at its end. (b) Restraint along one edge.

FIGURE 2.3: Types of restraint to walls. Figure adapted from Eurocode 2, Part 3, Annex M [4].

2.7.2 Restraint of a Member at its End

The maximum crack width may be calculated from the expression:

$$w_k = s_{r,max} \times (\varepsilon_{sm} - \varepsilon_{cm}) \tag{2.3}$$

where $s_{r,max}$ is the maximum crack spacing and $(\varepsilon_{sm} - \varepsilon_{cm})$ is the difference in deformation between steel and concrete over the maximum crack spacing.

For a member restrained at its end $(\varepsilon_{sm} - \varepsilon_{cm})$ may be calculated from the following expression:

$$\epsilon_{sm} - \epsilon_{cm} = \frac{0.5\alpha_e k_c k f_{ct,eff}}{E_s}(1 + \frac{1}{\alpha_e \rho}) \tag{2.4}$$

where

- α_e is the ratio E_s/E_{cm}
- k_c is a coefficient which takes account of the stress distribution within the section immediately prior to cracking and of the change of the lever arm.

- k is the coefficient which allows for the effect of non-uniform self-equilibrating stresses, which lead to a reduction of restraint forces.
- $f_{ct,eff}$ is the mean value of the tensile strength of the concrete effective at the time when the cracks may first be expected to occur.
- ρ is the ratio A_s/A_{ct}, where A_s is the reinforcement area and A_{ct} is the area of concrete in tension.

One may check cracking without direct calculation. This is done by calculating σ_s from the expression:

$$\sigma_s = \frac{k_c k f_{ct,eff}}{\rho} \tag{2.5}$$

2.7.3 Restraint Along One Edge

In case of restraint along one edge, the formation of a crack only influences the distribution of stresses locally, and the crack width is therefore a function of the restrained strain. The crack width may be estimated by the expression:

$$(\varepsilon_{sm} - \varepsilon_{cm}) = R_{ax}\varepsilon_{free} \tag{2.6}$$

where R_{ax} is a factor defining the degree of external restraint provided by elements attached to the element considered and ε_{free} is the strain which would occur if the member was completely unrestrained.

Figure 2.4 illustrates the difference between cracking in case of end and edge restraint.

2.8 Measures to Reduce Effects of Cracking

In this section it is discussed how to design concrete structures to reduce effects of cracking due to restraint of imposed deformations from thermal effects and shrinkage. All literature is obtained from a note written by Terje Kanstad, prepared as basis for a meeting in CEN WG1/TG7 Karlsruhe February 1 and 2, 2016: *Draft for Annex D for Eurocode 2 - 2020: Guidance to restrict early age cracking + Quotation of relevant crack width equations* (Revised February 26th 2016).

The most serious problem concerning both durability and serviceability is through-cracking. The amount of these cracks may, however, be reduced by performing some measures. Possible measures, presented in the draft, are to use low heat concretes, concretes with a low coefficient of thermal expansion, heating cables in the restraining structural elements, cooling pipes in the hardening concrete, reduced fresh concrete temperature, or finally to reduce the degree of restraint for the hardening concrete structural element.

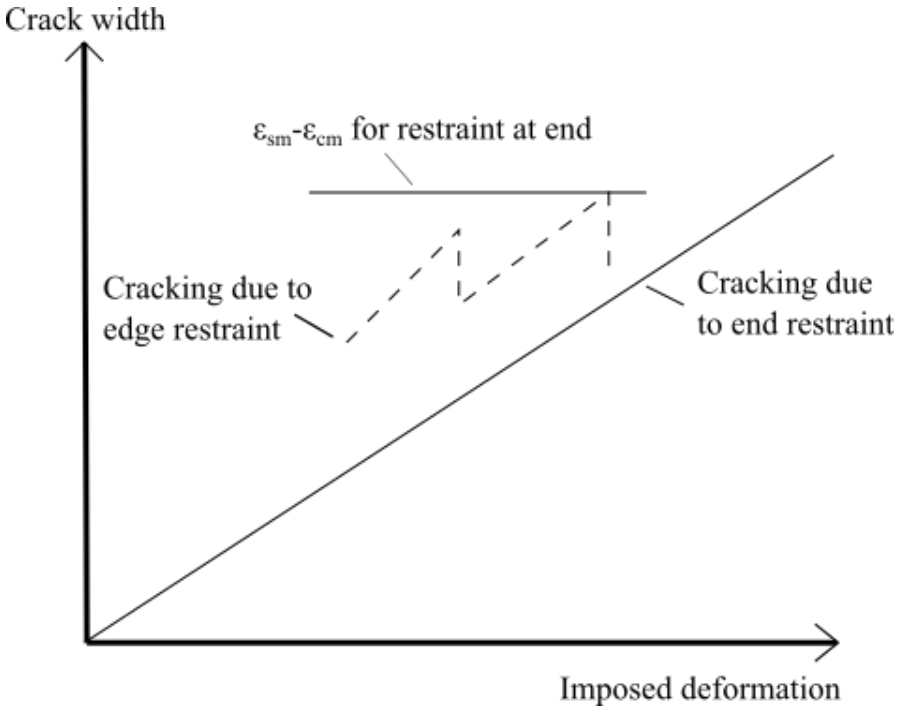

FIGURE 2.4: Relation between crack width and imposed strain for edge and end restrained walls. Figure adapted from Eurocode 2, Part 3, Annex M [4].

Figure 2.5(a) illustrates the expansion phase corresponding to the heating phase, while Figure 2.5(b) shows the contraction phase which is an effect of the cooling. Both figures also illustrate the typical distribution of stresses over the wall height. The most critical time for cracking, t_{crit}, is usually assumed to be when the wall temperature reaches the temperature of the surroundings.

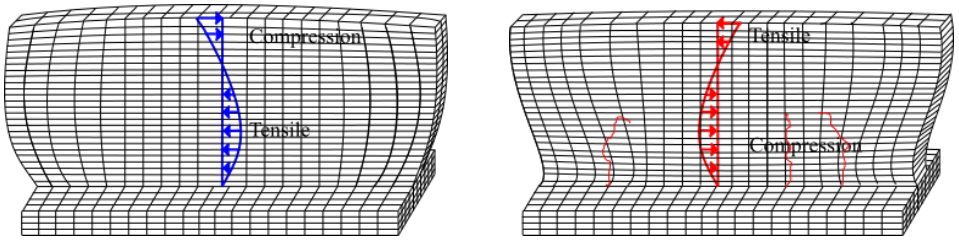

(a) Concrete wall in expansion phase.

(b) Concrete wall in contraction phase.

FIGURE 2.5: Illustration of the expansion and contraction phase in a wall, as well as the stress distribution. Figure adapted from *Draft for Annex D for Eurocode 2 -2020.*

Related to temperature development in the hardening concrete, the most decisive parameters are the fresh concrete temperature, T_{ci}, and the ambient temperature history. In addition, also the insulation conditions of the surface of the member, the wind conditions and the solar radiation influence the concrete temperature history. To describe temperature history, the fresh concrete temperature, the maximum concrete temperature and the temperature of the surroundings have

to be considered. To obtain a complete crack assessment, also the minimum temperatures due to the seasonal variations must be determined, both for exposed and restraining structures.

Reinforcement may reduce crack spacing and limit the crack widths, but it cannot, however, prevent early age cracking. The imposed load effects related to early age cracking are often membrane actions, as for through cracking, or simply local effects, such as surface cracking. These differ from the load effects presumed in the minimum reinforcement rules, and are hence a complicated problem for designers. The minimum reinforcement rules generally relate to cross section behavior with linear strain distribution, which in general does not hold in massive concrete structures, where early age cracking problems may occur.

It has been assumed that limiting the temperature differences across the cross-section of a member to 20°C, or between a hardening and a restraining member to 15°C, will give a structure without early age cracking. These are very rough requirements, and they are solely connected to temperature and obviously insufficient on a fundamental level since the other parameters involved are not considered.

Considering prevention or limitation of cracking due to imposed deformations by strain and stress calculations, the methods may be grouped into three levels:

(I) Simple conservative methods with default values

(II) Reasonably simple methods with representative input parameters

(III) Advanced timedependent FE Analyses for temperatures, strains and stresses.

2.9 Early-age Thermal Crack Control in Concrete

2.9.1 General

In this section a procedure for controlling early-age thermal cracking is presented. The theory is obtained from the British guideline *Early-age thermal crack control in concrete - CIRIA C660* [9]. During hydration of concrete, heat is released from the clinker, which may cause early-age thermal cracking. When the tensile strain, arising from either restrained thermal contraction or a temperature differential within the concrete, exceeds the tensile strain capacity, early-age thermal cracking occurs. Autogenous shrinkage may also contribute to early contraction. In thin sections, early-age thermal cracking may occur within a few days. Some of the factors that influence the risk of early-age thermal cracking are listed below.

- Temperature rise
- The coefficient of thermal expansion of the concrete
- The restraint to movement offered by adjacent elements
- The restraint to movement offered by differential strain within an element

- The ability of the concrete to resist tensile strain

External restraint may be in two principal forms, either continuous edge restraint or end restraint. In the case with edge beams on a bridge, it is edge restraint that is the restraint case.

The temperature rise in the concrete depends on the capacity of the concrete to generate heat, depending on content and type of cement, the element thickness and the curing conditions.

2.9.2 The Design Process

The steps involved in the design process for assessing and controlling early age cracking are listed below.

1. Define the allowable crack width
2. Define the nature and magnitude of restraint
3. Estimate the magnitude of restrained strain and the risk of cracking
4. Estimate the crack-inducing strain
5. Check the minimum area of reinforcement $A_{s,min}$
6. Check the reinforcement for crack control, crack spacing and width

2.9.3 Allowable Crack Width

It is not common practice to add early-age crack widths to the crack widths arising from structural loading. Nevertheless, the designer should consider whether or not to add cracking due to subsequent deformations to the early-age effects. Depending on the restraint, long-term thermal contractions and drying shrinkage may either cause crack widths to increase or new cracks to form.

If a member is subjected to continuous edge restraint and the restraint is maintained, one may expect the cracks that are formed at a early age to widen. If both the retained and the restraining member are exposed to the same environment, only the differential deformation needs to be considered when estimating the crack widening.

In members subjected to end restraint, the crack width is determined by the strength of the concrete at the time of cracking. As the strength develops, the restrained contraction will increase the existing crack widths and cause new cracks to form. These cracks are wider than the early-age cracks.

The crack width is given by the expression:

$w_k = S_{r,max}(\varepsilon_{sm} - \varepsilon_{cm})$

where $S_{r,max}$ is the maximum crack spacing, as shown in Figure 2.6, ε_{sm} is the mean strain in the reinforcement and ε_{cm} is the mean strain in the concrete between cracks.

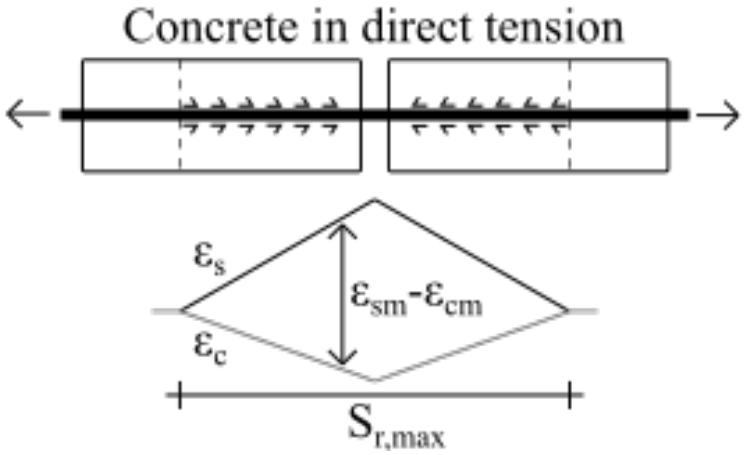

FIGURE 2.6: Illustration of maximum crack spacing in reinforced concrete.

2.9.4 Nature and Magnitude of Restraint

The restraint plays an important role in determining the restrained strain and risk of cracking. If the restraint is low, early thermal cracking may be avoided, and hence also the early thermal cracking control. If cracking is predicted, the nature of restraint (end or edge) has a significant impact on the amount of reinforcement needed.

In some cases the restraining members may be subject to a greater risk of cracking than the newly cast member.

2.9.5 The Magnitude of Restrained Strain and the Risk of Cracking

The risk of cracking should be evaluated in two different cases: Both when early temperature change and autogenous shrinkage will be the major cause of strain during the early period, and later when temperature changes and drying shrinkage will dominate.

If the cracking that has developed in the early period is unacceptable, one must consider the options for reducing the restraint and/or the thermal strain.

If the risk of cracking is acceptable low, then there is no need to design or to check reinforcement specifically to control cracking caused by restrained contraction.

2.9.6 Crack-inducing Strain

Eurocode 2, Part 3 defines the crack-inducing strain as the difference between the mean strain in the reinforcement and the mean strain in the concrete after a crack has occurred [4]. In case

of restraint of a member at its ends, as shown in Figure 2.7(a), the crack-inducing strain is given by the expression:

$$\varepsilon_{sm} - \varepsilon_{cm} = \frac{0.5\alpha_e k_c k f_{ct,eff}}{E_s}\left(1 + \frac{1}{\alpha_e \rho}\right) \tag{2.7}$$

where

- k is a coefficient which allows for the effect of non-uniform and self-equilibrating stress which leads to a reduction in restraint forces
- k_c is a coefficient which takes account of the stress distribution within the section immediately prior to cracking
- $f_{ct,eff}$ is the mean tensile strength of the concrete at the time of cracking
- E_s is the modulus of elasticity of the reinforcement
- α_e is the modular ratio
- ρ is the ratio A_s/A_{ct}
- A_s is the total area of reinforcement
- A_{ct} is the gross section in tension

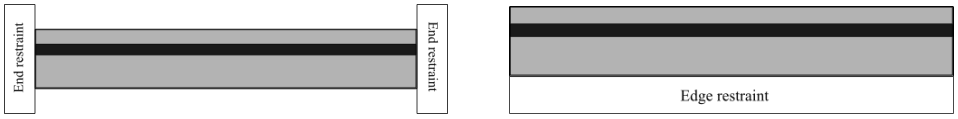

(a) End restraint (b) Edge restraint

FIGURE 2.7: The difference between edge and end restraint. Figure adapted from *Early-age thermal crack control in concrete* [9].

In case of edge restraint, illustrated in Figure 2.7(b), the crack-inducing strain is given by the expression:

$$\varepsilon_{sm} - \varepsilon_{cm} = R_{ax}\varepsilon_{free} \tag{2.8}$$

where

- R_{ax} is the restraint factor
- ε_{free} is the strain which would occur if the member was completely unrestrained

2.9.7 Minimum Area of Reinforcement

Eurocode 2, Part 1-1 presents an expression for the minimum area of reinforcement, which ensures that the reinforcement doesn't yield under the load transferred from the concrete to the steel when a crack occurs [8]. For members subjected to continuous edge restraint, this expression is over-conservative. It has therefore been modified for this case:

$$A_{s,min} = k_{Redge} k_c A_{ct} \frac{f_{ckt,0.05}(t)}{f_{yk}} \tag{2.9}$$

where $f_{ckt,0.05}$ is 70% of the mean axial tensile strength , f_{yk} is the characteristic yield strength of the reinforcement, and k_{Redge} is conservatively calculated from the expression:

$$k_{Redge} = 1 - 0.5 \times R_{edge} \tag{2.10}$$

where R_edge is the edge restraint factor at the location of the maximum crack width.

2.9.8 Check the Reinforcement for Crack Control, Crack Spacing and Width

If the estimated crack width exceeds the upper limit, one may consider options to reduce the extent of cracking, for example by increasing the amount of reinforcement.

If the elements are subjected to edge restraint, the crack width is strain limited and may be reduced by achieving less restrained thermal strain. For the end restraint case, on the other hand, a decrease in thermal strain will only reduce the number of cracks, not the crack width. In this case one should rather decrease the restraint or increase the amount of reinforcement.

[9]

Chapter 3

Models for Crack Width Calculation

In this chapter three different methods for calculating the crack width in concrete are presented. First a calculation method for crack widths in structures with combined reinforcement is presented. That is structures containing both ordinary reinforcement bars and fiber reinforcement. The second model that is presented is a calculation model for crack widths in structures exposed to shrinkage cracking in fully restrained members. Lastly, a method for early-age thermal crack control is presented.

3.1 Calculation of Crack Widths in Structures with Combined Reinforcement

This section is influenced by the paper presented at Nordic Mini-seminar "Fiber reinforced concrete", *Calculation of crack width and crack spacing*, written by Ingemar Löfgren [2].

Löfgren states that almost no guidelines exist for structural engineers concerning structures having both fibre- and bar reinforcement. If cracking is caused by an imposed deformation, the force in the member depends on the actual stiffness and the crack width on the number of cracked formed. Engström [10] has proposed a model for analysing restraint induced cracking in concrete with ordinary bar reinforcement. The cracking process is analysed by modeling the reinforcement in the cracks as non-linear springs, illustrated in Figure 3.1. Löfgren has extended the model to also include the effect of fibre reinforcement. This model is presented in this section.

Löfgren's model shows how the combined effect of bar reinforcement and fibre bridging influences the crack spacing and width in the serviceability limit state. Figure 3.2 illustrates how forces are acting on un-cracked parts of concrete with both fiber reinforcement and ordinary reinforcement bars. The model is only valid for cracking caused by restraint stresses. It is based on a bond-slip relationship between reinforcement and concrete, as well as a compatibility requirement for the combined material.

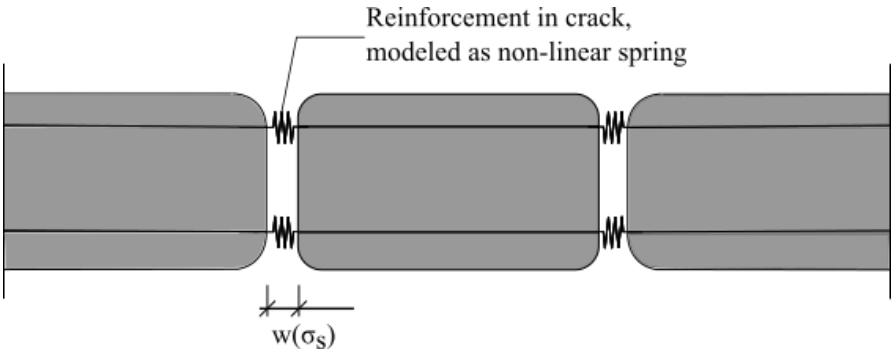

FIGURE 3.1: The reinforcement in the cracks modelled as non-linear springs [2].

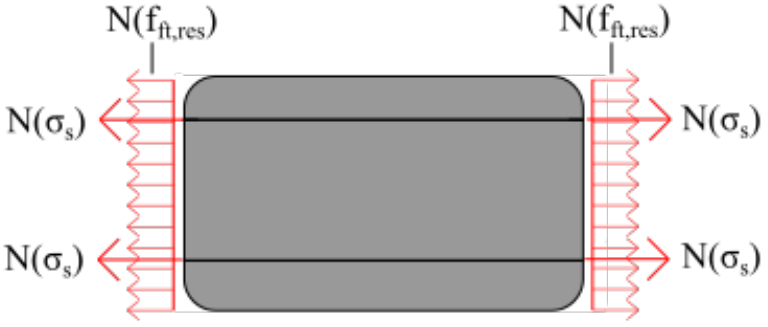

FIGURE 3.2: Forces acting on an un-cracked concrete with combined reinforcement[2].

Based on a bond-slip relationship an analytical expression has been derived, describing the crack width as a function of the reinforcement stress

$$w(\sigma_s) = 0.42\left(\frac{\phi \times \sigma_s^2}{0.22 \times f_{cm} E_s \left(1 + \frac{E_s}{E_c} \times \frac{A_s}{A_{ef}}\right)}\right) \tag{3.1}$$

where

- ϕ is the bar diameter
- σ_s is the stress in the reinforcement
- f_{cm} is the average compressive concrete strength
- E_s and E_c is the modulus of elasticity of the reinforcement respectively the concrete
- A_{ef} is the effective concrete area

The effective concrete area is calculated as $A_{ef} = b \times h_{ef}$, where h_{ef} is the part of the tensile zone which has the same centre of gravity as the reinforcement.

The response during the cracking process may be described with the following deformation criteria:

$$\frac{N(\sigma_s, f_{ft,res}) \times l}{E_c \times A_I}(1 + \phi_{ef}) + n \times w(\sigma_s) = R \times \epsilon_{cs} \times l \tag{3.2}$$

where

- $N(\sigma_s, f_{ft,res})$ is the force acting on un-cracked parts
- l is the length of the member
- $A_I = A_c + A_s(\frac{E_s}{E_c} - 1)$
- ϕ_{ef} is the effective creep coefficient
- n is the number of cracks
- R is the degree of restraint, where $R = 0$ for no restraint and $R = 1$ for full restraint

$N(\sigma_s, f_{ft,res})$ may be calculated as:

$$N(\sigma_s, f_{ft,res}) = \sigma_s \times A_s + f_{ft,res}(A_{ef} - A_s) \tag{3.3}$$

If $N(\sigma_s, f_{ft,res})$ is larger than the force required to initiate a new crack, N_1, more cracks will be formed. However, if it is smaller only one crack will be formed. The force required to initiate a new crack, N_1, can be calculated as:

$$N_1 = f_{ctm}\Big(A_{ef} + \Big(\frac{E_s}{E_c} - 1\Big)\Big) \tag{3.4}$$

where f_{ctm} is the average tensile strength.

If $N_(\sigma_s, f_{ft,res}) > N_1$ a new crack is initiated and n increases. If $N_(\sigma_s, f_{ft,res}) < N_1$ the cracking process stops and the actual crack width can be determined using equation 3.1.

[2]

3.2 Shrinkage Cracking in Fully Restrained Members

In this section the problem of cracking in fully restrained members subjected to direct tension caused by drying shrinkage is considered. A rational approach for determination of number and spacing of cracks, as well as the average crack width are presented. The approach is obtained from ACI Structural Journal, Vol.89 no.2 [11].

3.2.1 Calculation of Restraining Force and Internal Stresses

To determine the crack width w and the stresses, the distance s_0 has to be known. s_0 is the distance over which the concrete and steel stresses vary. Further on, the restraining force, N_{cr}, has to be calculated. The stress in the concrete varies from zero at the crack, to compressive stress, σ_{c1} at $x = s_0$. The stress in the steel varies from the tensile stress, σ_{s2}, to the compressive stress, σ_{s1}, at $x = s_0$.

An approximation for s_0 may be obtained from the following equation:

$$s_0 = \frac{d_b}{10\rho} \tag{3.5}$$

where d_b is the bar diameter and ρ is the reinforcement ratio A_s/A_c.

The following procedure shows how to calculate N_{cr} immediately after the first cracking, as well as the corresponding stresses. Since the member is fully restrained, it is prevented from shortening, and hence the overall elongation of the steel is zero. Integrating the steel strain over the length of the member gives:

$$\frac{\varepsilon_{s1}}{E_s}L + \frac{\sigma_{s2} - \sigma_{s1}}{E_s}\left(\frac{2}{3}s_0 + w\right) = 0 \tag{3.6}$$

Since w is much less than s_0, w can be neglected. A rearrange of Equation 3.6 gives:

$$\sigma_{s1} = \frac{-2s_0}{3L - 2s_0}\sigma_{s2} \tag{3.7}$$

At the crack the restraining force is carried entirely by the steel, which gives the equation for the stress at the crack as:

$$\sigma_{s2} = \frac{N_{cr}}{A_s} \tag{3.8}$$

The steel stress away from the crack is given by substituting Equation 3.8 into Equation 3.7:

$$\sigma_{s1} = \frac{2s_0}{3L - 2s_0}\frac{N_{cr}}{A_s} = -C_1\frac{N_{cr}}{A_s} \tag{3.9}$$

where

$$C_1 = -\frac{2s_0}{3L - 2s_0} \tag{3.10}$$

Because the member is fully restrained, the total concrete strain is zero at any point prior to cracking. The creep and elastic strains are tensile and the shrinkage strain is compressive (negative). Immediately before the first crack occurs, the sum of the creep and the shrinkage strain components is

$$\varepsilon_c + \varepsilon_{sh} = -\frac{f_t}{E_c} \tag{3.11}$$

where f_t is the concrete stress and E_c is the elastic modulus of the concrete at the time of first cracking. Immediately after first cracking, the magnitude of the elastic component of strain in the uncracked concrete decreases, but the creep and shrinkage strain components are unaltered.

At any distance greater than s_o from the crack, equilibrium requires that the sum of the forces in the concrete and the steel immediately after first cracking is equal to N_{cr}.

$$\sigma_{c1}A_c + \sigma_{s1}A_s = N_{cr} \tag{3.12}$$

Substituting Equation 3.9 into Equation 3.12 and rearranging gives

$$\sigma_{c1} = \frac{N_{cr} - \sigma_{s1}A_s}{A_c} = \frac{N_{cr}(1 + C_1)}{A_c} \tag{3.13}$$

The compatibility requirement is that the concrete and steel strains at any distance greater than s_0 from the crack, are identical. That is

$$\epsilon_{s1} = \epsilon_1 \tag{3.14}$$

which can be expressed as

$$\frac{\sigma_{s1}}{E_s} = \frac{\sigma_{c1}}{E_c} + \epsilon_c + \epsilon_{sh} \tag{3.15}$$

Substituting Equation 3.9, 3.11 and 3.13 into Equation 3.15 and solving for N_{cr} gives

$$N_{cr} = \frac{\eta\rho f_t A_c}{C_1 + \eta\rho(1 + C_1)} \tag{3.16}$$

where $\rho = \frac{A_s}{A_c}$ and $\eta = \frac{E_s}{E_c}$. When N_{cr} is calculated, the concrete and steel stresses immediately after cracking may be calculated from from Equation 3.8, 3.9 and 3.13.

3.2.2 Calculation of Final Stresses and Deformation

The final stresses and deformation are indicated with an asterisk(*). By equating the overall elongation of the steel to zero, the following expression for a member containing m cracks is obtained:

$$\frac{\sigma^*_{s1}}{E_s}L + m\frac{\sigma^*_{s2} - \sigma^*_{s1}}{E_s}(\frac{2}{3}s_0 + w) = 0 \tag{3.17}$$

The crack width w is much less than s_0, and can therefore be neglected. Rearranging the above equation gives the following expression

$$\sigma^*_{s1} = \frac{-2s_0 m}{3L - 2s_0 m}\sigma^*_{s2} \tag{3.18}$$

Letting the crack spacing s = $\frac{L}{m}$ gives

$$\sigma_{s1}^* = \frac{-2s_0}{3s - 2s_0}\sigma_{s2}^* = -C_2\sigma_{s2}^* \tag{3.19}$$

where

$$C_2 = \frac{2s_0}{3s - 2s_0} \tag{3.20}$$

The final tensile stress in the reinforcement at each crack is:

$$\sigma_{s2}^* = \frac{N(\infty)}{A_s} \tag{3.21}$$

The concrete stress history is continuously changing, but it is yet reasonable to assume that the average concrete stress for the estimation of creep strain at any time after the commencement of drying, σ_{av}, is somewhere between σ_{c1} and f_t. An approximation of the final creep strain is given by:

$$\epsilon_c^* = \frac{\sigma_{av}}{E_c}\phi^* \tag{3.22}$$

where ϕ^* is the final creep coefficient. It is assumed that

$$\sigma_{av} = \frac{\sigma_{c1} + f_t}{2} \tag{3.23}$$

At any distance greater than s_o from the crack, the final concrete strain is the sum of the elastic, creep and shrinkage components and may be approximated by:

$$\epsilon_1^* = \epsilon_e + \epsilon_c^* + \epsilon_{sh}^* = \frac{\sigma_{av}}{E_c} + \frac{\sigma_{av}}{E_c}\phi^* + \epsilon_{sh}^* = \frac{\sigma_{av}}{E_e^*} + \epsilon_{sh} \tag{3.24}$$

where

$$E_e^* = \frac{E_c}{1 + \phi^*} \tag{3.25}$$

The final creep coefficient depends on the age at the commencement of drying and the quality of the concrete, and is normally between 2 and 4. ϵ_{sh}^* is the final shrinkage strain and depends on the relative humidity, the size and shape of the member and the characteristics of the concrete mix.

At any distance greater than s_o from the crack, equilibrium requires that the sum of the force in the concrete and the force in the steel is equal to $N(\infty)$. That is:

$$\sigma_{c1}^* A_c + \sigma_{s1}^* A_s = N(\infty) \rightarrow \sigma_{c1}^* = \frac{N(\infty) - \sigma_{s1}^* A_s}{A_c} \tag{3.26}$$

Compatibility gives that the concrete and steel strains are identical:

$$\epsilon_{s1}^* = \epsilon_1^* \tag{3.27}$$

This gives:

$$\frac{\sigma_{s1}^*}{E_s} = \frac{\sigma_{av}}{E_c^*} + \epsilon_{sh} \tag{3.28}$$

Substituting Equation 3.19 and 3.21 into Equation 3.28 gives:

$$N(\infty) = -\frac{n^* A_s}{C_2}(\sigma_{av} + \epsilon_{sh}^* E_e^*) \tag{3.29}$$

where $n^* = E_s/E_e^*$.

The crack spacing must be determined to calculate C_2. σ_{c1} must be less than the tensile strength f_t. Substituting Equation 3.19 and 3.21 into Equation 3.26, combined with the tensile strength criteria gives:

$$\sigma_{c1}^* = \frac{N(\infty)(1 + C_2)}{A_c} \leqslant f_t \tag{3.30}$$

Substituting Equation 3.20 and 3.29 into Equation 3.30 gives:

$$s \leqslant \frac{2s_o(1 + \xi)}{3\xi} \tag{3.31}$$

where

$$\xi = \frac{-n^* \rho(\sigma_{av} + \epsilon_{sh}^* E_e^*)}{n^* \rho(\sigma_{av} + \epsilon_{sh}^* E_e^*) + f_t} \tag{3.32}$$

The number of cracks m may be taken as the smallest integer that satisfies equation 3.31. Then the restraining force can be calculated using equation 3.29. The steel and the concrete stresses may be determined from equation 3.21.

The overall shortening of the concrete is an estimate of the sum of the crack widths. The final concrete strain at any distance less than s_o from the crack is:

$$\epsilon_2^* = \frac{f n \sigma_{c1}^*}{E_e^*} + \epsilon_{sh}^* \tag{3.33}$$

If a parabolic variation of stress in the region less than a distance s_o away from the crack is assumed, the average crack width w is obtained by integrating the concrete strain over the length of the member.

$$w = -\left[\frac{\sigma^*_{c1}}{E^*_e}(s - \frac{2}{3}s_0) + \epsilon^*_{sh}s\right] \tag{3.34}$$

If the area of steel, A_s is small, yielding may occur at each crack and the value of $N(\infty)$ will not be correct. In such case $N(\infty)$ is equal to $f_y A_s$. The stress in the concrete at any distance greater than s_o from the crack is then:

$$\sigma^*_{c1} = \frac{f_y A_s - \sigma^*_{s1} A_s}{A_c} \tag{3.35}$$

After the steel at the first crack yields, the tensile stress σ_{c1} increases only slightly in the concrete, as the compressive steel stress σ_{s1} increases with time and the first crack opens. The width of the crack is usually unacceptably large as the steel at the crack deforms plastically. The crack width w may be found by insuring that the overall elongation of the steel is zero. That is:

$$\frac{\sigma^*_{s1}}{E_s}(L - w) + \frac{f_y - \sigma^*_{s1}}{E_s} \times \frac{2}{3}s_0 + w = 0 \tag{3.36}$$

Since w is much smaller than L, equation 3.36 can be arranged to:

$$w = -\frac{\sigma^*_{s1}(3L - 2s_0) + 2s_0 f_y}{3E_s} \tag{3.37}$$

Since the tensile stress in the uncracked concrete does not change significantly with time, it is reasonable to assume that the average concrete stress, σ_{av}, is given by equation 3.35 and that the final steel stress at any distance greater than s_o from the first crack may be obtained by substituting equation 3.35 into equation 3.24 and simplifying:

$$\frac{\sigma^*_{s1}}{E_s} = \frac{f_{sy} A_s - \sigma^*_{s1} A_s}{A_c E^*_e} \rightarrow \sigma^*_{s1} = \frac{n^* \rho f_{sy} + \epsilon^*_{sh} E_s}{1 + n^* \rho} \tag{3.38}$$

3.3 Early-age Thermal Crack Control in Concrete

The calculation model presented in this section is obtained from the British guideline *Early-age thermal crack control in concrete - CIRIA C660* [9]. Extensive theory about the model is presented in Section 2.9.

The allowable crack width is determined from the requirement of a durable concrete structure. The limiting total crack width arising from early-age deformations, long-term deformations and loading, is 0.3 mm. The full crack pattern is expected to occur at early age under conditions of edge restraint.

To calculate the edge restraint, the restraint at the joint is first estimated, R_j, according to the equation:

$$R_j = \frac{1}{1 + \frac{A_n}{A_0} \times \frac{E_n}{E_0}} \tag{3.39}$$

where

- A_n is the cross-sectional area of the new (restrained) pour
- A_o is the cross-sectional area of the old (restraining) concrete
- E_n is the modulus of elasticity of the new pour concrete
- E_o is the modulus of elasticity of the old concrete

R_1 is the restraint factor that applies during the early thermal cycle. R_2 and R_3 are restraint factors applying to medium and long-term deformation and drying shrinkage respectively.

In the early thermal cycle, the modulus of elasticity will be less developed in the newly cast concrete, compared to the old concrete. It therefore is recommended to use a ratio of $E_0/E_n = 0.7 - 0.8$ in the early age.

Restrained strain is expressed as

$$\varepsilon_r = K_{c1}[\alpha_c T_1 + \varepsilon_{ca(3)}]R_1 + K_{c2}[(\varepsilon_{ca(28)} - \varepsilon_{ca(3)})R_2 + \alpha_c T_2 R_3 + \varepsilon_{cd} R_3] \tag{3.40}$$

where $K_{c1} = 0.65$ and $K_{c2} = 0.5$.

T_1 is the difference between the peak temperature, T_p, and the mean ambient temperature, T_a, at the end of the thermal cycle.

To predict T_1, the cement content is required. While a reduction in the heat generation of the binder is likely to be beneficial, it is the temperature rise in the resulting concrete that is of principal concern with regard to early thermal cracking. When additions are used, different binder contents are often required to achieve the same strength class of concrete and it is important that this is taken into account when assessing the benefits or otherwise of a particular mix design.

Values of T_1 for CEM II for walls cooling from both faces are given in Figure 9.1. The British guideline presents a table where the total binder content is given for different strength classes, *Table 4.2*.

T_2 is the difference between the mean ambient temperature at the end of the early thermal cycle and the minimum element temperature likely in the course of the element life. For annual temperature changes recommended values of T_2 are 20 °C for concrete cast in the summer and 10 °C for concrete cast in the winter.

The autogenous shrinkage is obtained from *Table 4.5*, presented in the British guideline, while the drying shrinkage is calculated from Eurocode 2, 3.1.4 (6).

t_s is the age of the concrete in days at the beginning of drying. This is normally at the end of the curing period. t is the age of the concrete at the given time.

The tensile strain capacity is given by the expression:

$$\varepsilon_{ctu}(ea) = 1.08\frac{f_{ctm}(3)}{E_{cm}(3)} \tag{3.41}$$

where f_{ctm} and E_{cm} is calculated from Eurocode 2, 3.1.2(9) and 3.1.3(3).

The crack-inducing strain for continuous edge restraint is estimated from the equation:

$$\varepsilon_{cr} = K_{c1}[\alpha_c T_1 + \varepsilon_{ca(3)}]R_1 + K_{c2}[(\varepsilon_{ca(28)} - \varepsilon_{ca(3)})R_2 + \alpha_c T_2 R_3 + \varepsilon_{cd}R_3] - 0.5\varepsilon_{ctu} \tag{3.42}$$

The crack width is then calculated from the formula:

$$w_k = S_{r,max}(\varepsilon_{sm} - \varepsilon_{cm}) = \varepsilon_{cr}\Big(3.4c + 0.425\frac{k_1 k_2 \phi}{\rho_{p,eff}}\Big) \tag{3.43}$$

Chapter 4

Laboratory Experiment

During the summer 2015, a laboratory experiment was performed in connection with the specialization project written by the undersigned. The purpose of the experiment was to provoke cracks in the early phase, and then study the effect on cracking of different fiber reinforcements. The cracks occurred due to external restraint, briefly explained in Section 1.1.

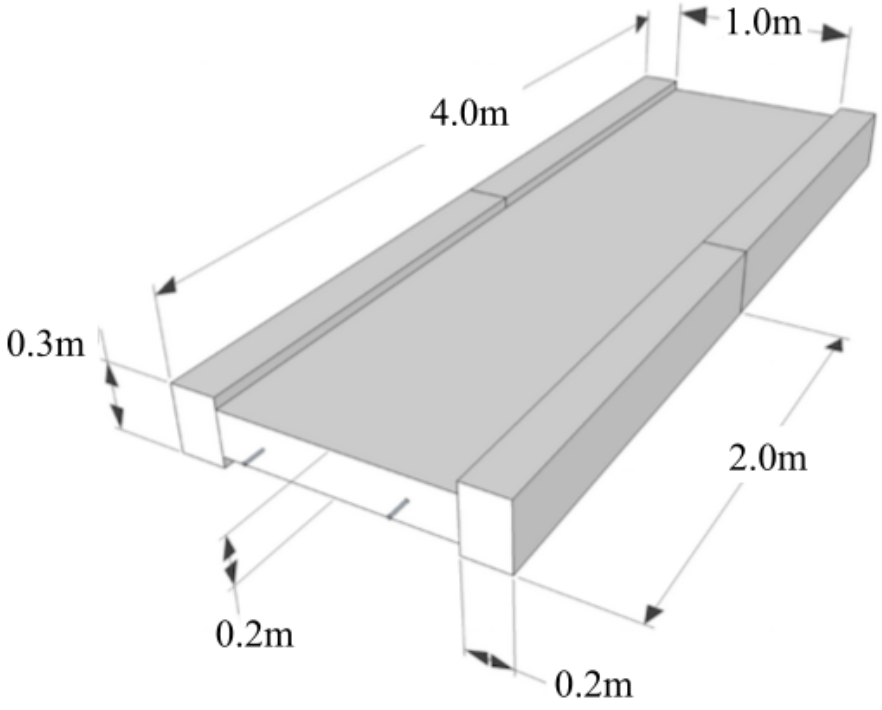

FIGURE 4.1: Dimensions of the slab and the edge beams that were cast in the laboratory experiment.

A concrete slab with dimensions $1 \times 4 \times 0.2$ meters was cast, see Figure 4.1. When the concrete temperature had dropped to the ambient temperature, four edge beams were cast, all with the same amount of traditional reinforcement bars. The reinforcement drawing of the beams and the slab is shown in Figure 4.2. The edge beams had the dimensions $0.2 \times 2 \times 0.3$ meters. Three of

the four concrete mixes were fiber mixes, with 0.5 % basalt fibers, 0.7 % polymer fibers and 0.4% steel fibers. During casting of the steel fiber mix, something went wrong, leading to a porous and damaged concrete surface. Hence this beam was rejected, and a new steel fiber beam was cast, where the basalt fiber beam was to be. There are therefore no results from the basalt fiber mix.

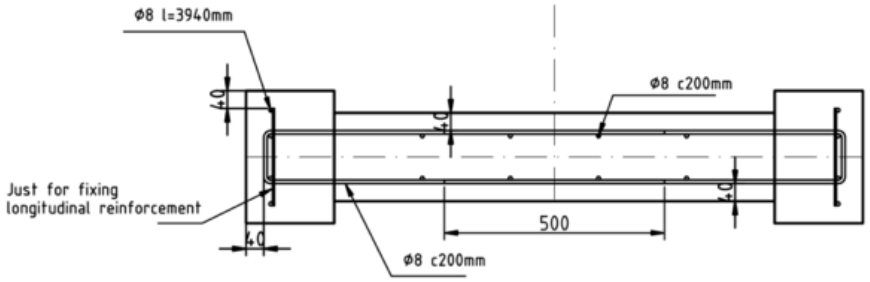

FIGURE 4.2: The placement and dimensions of the reinforcement in the laboratory experiment.

Heating cables were installed in the slab, to increase the temperature difference between the slab and the edge beam. To maximize the temperature difference, the edge beams were insulated during curing, while the slab was insulated during heating. The temperature development was plotted as a function of time, and it was performed accurate crack mappings regularly during the experiment.

The temperature development is shown in Figure 4.3 and Figure 4.4. The maximum temperature difference between the edge beam and the slab during the hardening phase equals 16 °C, while the maximum temperature difference that occurred during heating of the slab equals 34 °C.

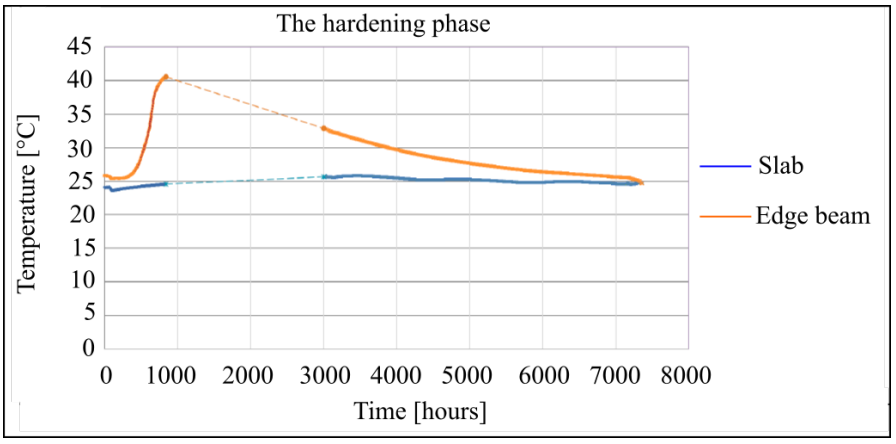

FIGURE 4.3: The temperature development in the slab and the edge beam during the hardening phase.

Average crack widths and crack spacings from the experiment are presented in Table 4.1. The average crack spacings are calculated by dividing the length of the edge beam by all observed cracks on the given beam. It should be kept in mind that the restraint is decreasing towards the ends of the beam, and hence these crack spacings may not be representative for the fiber mixes. However, the values may be used as basis for comparison of the effect of the fiber types, since all values are calculated on the same conditions.

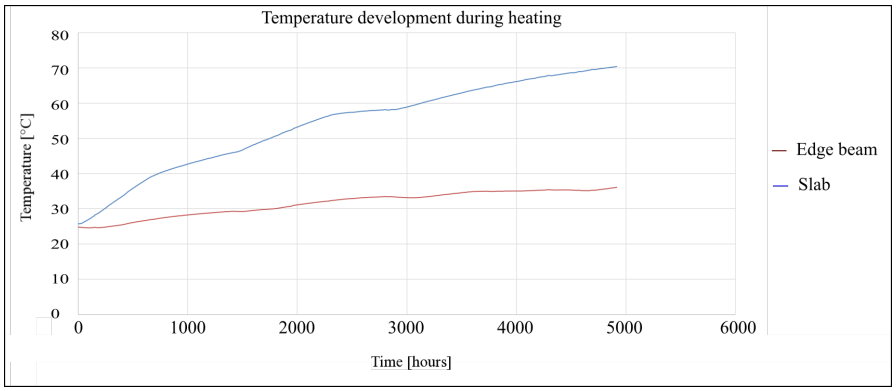

FIGURE 4.4: The temperature development in the slab and the edge beam during heating of the slab.

TABLE 4.1: Results from the laboratory experiment.

Concrete mix	Average crack width [mm]	Average crack spacing [mm]
Reference mix	0.17	286
Polymer fiber mix	0.06	133
Steel fiber mix	0.04	100

The table illustrates the positive effect fiber reinforcement has on the crack development. In the fiber mixes, a much denser crack development is observed, than for the reference concrete, and the crack widths are much smaller in the fiber mixes. The steel fibers reduced the average crack width by a factor of 4-5, while the polymer fibers reduced the crack width by a factor of 2-3.

The final crack mapping for each beam, that was performed when the heating cables were turned off, is shown are Figure 4.5, 4.6 and 4.7. In the reference beam, it is only observed a few cracks with larger crack widths than for the fiber beams.

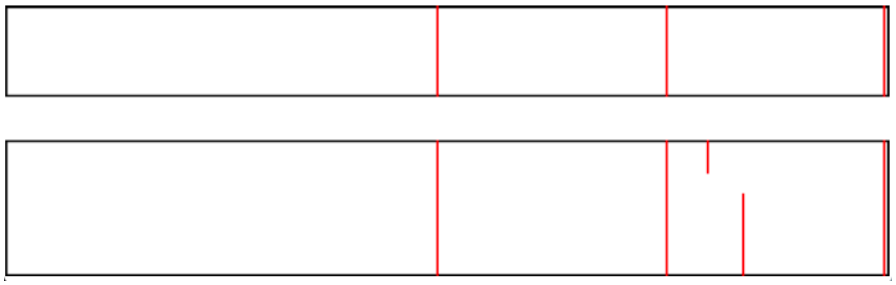

FIGURE 4.5: The final crack mapping of the reference beam, modeled in AutoCAD.

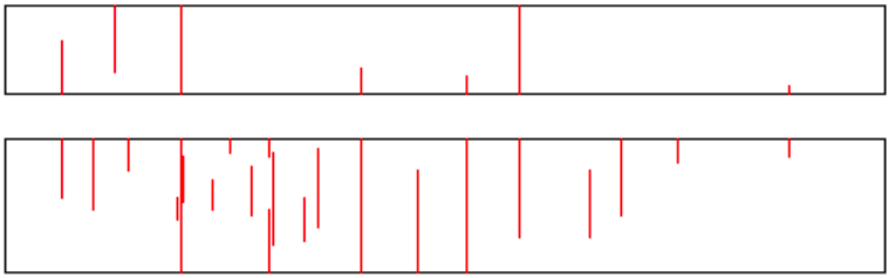

FIGURE 4.6: The final crack mapping of the steel fiber beam, modeled in AutoCAD.

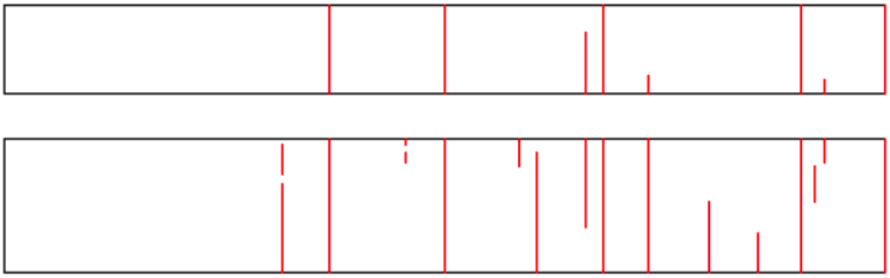

FIGURE 4.7: The final crack mapping of the polymer fiber beam, modeled in AutoCAD.

Chapter 5

Construction Site Visit

5.1 Sandsgård Bridge

March 16 and 17, 2016, the author visited a construction site in Sandnes, where the edge beams of Sandsgård Bridge were cast. The bridge is shown in Figure 5.1. The two edge beams were divided into three sections each, and the in total six sections à 16 m were cast from different types of fibre concrete.

FIGURE 5.1: Photography of Sandsgård bridge rigth before casting of the edge beams.

The different types of fibre concrete that were used are:

- Reference concrete with ordinary reinforcement bars
- Concrete with ordinary hooked end steel fibers: 40 kg/m^3, L/d = 50/1.0 = 50

- Concrete with ReforceTech Minibar (basalt fiber), product number 34317 PC: 12 kg/m^3, L/d = 43/0.65 = 66.2
- Concrete with polymer fibers M50: 8 kg/m^3, L/d = 50/1.1 = 45.5
- Concrete with galvanized steel fibers: 35 kg/m^3, L/d = 50/0.75 = 67
- Concrete with stainless steel fibers 35 kg/m^3, L/d = 50/0.75 = 67

March 16, 2016, the temperature sensors were installed in the six different edge beams. The sensors were placed in the center of the beams. They were insulated with tape to avoid electrical contact with the reinforcement.

March 17, 2016, the edge beams were cast. Before casting of the beams, trial mixes of the reference concrete and the steel fiber concrete were cast. It was not performed trial mixes of the other fiber mixes.

Before casting, the air content and temperature of each concrete mix were measured, as well as the ambient temperature. The measured values are shown in Table 5.1.

TABLE 5.1: Measured air content and temperatures for each concrete mix.

Concrete mix	Air content [%]	Concrete temperature [C°]	Ambient temperature [C°]
Reference concrete	3.8	11.4	3.5
Ordinary steel fibers	4.0	13.5	8.9
Basalt fibers	2.6	16.7	12.3
Polymer fibers	5.8	17.6	12.8
Galvanized steel fibers	3.0	15.9	12.0
Stainless steel fibers	4.0	13.5	8.0

First the reference concrete was cast, and then the concrete with ordinary steel fibers was cast. The third mix that was cast was the concrete with polymer fibers. During casting of this beam, a plug formed in the pump, as shown in Figure 5.2. By that time, about 4 length meters of the edge beam were cast. To avoid that another plug should form, the polymer fiber mix was thrown away, and the concrete mix with basalt fiber was cast in the rest of the beam. A new polymer mix was cast on the fourth beam, where the amount of fibers was reduced from $8kg/m^3$ to $4kg/m^3$, purposely to increase the pumpability of the concrete.

The fifth and sixth beam were respectively cast from the concrete mixes with galvanized steel and stainless steel fibers. During casting of the mix with galvanized steel fibers another plug arose in the pump. This plug was not formed due to the properties of the mix, but arose due to worn pumping equipment. A bolt came loose from the pump, and created a plug in the concrete. Due to this another pumping pipe was hired.

During the stops, both for the polymer fiber and the galvanized fiber mix, the mixes were vibrated to delay the curing, while waiting for further casting. Figure 5.3 shows the location of the different parts where the different mixes were used, from northwest(left) to southeast(right). All of the concretes had the same recipes, except for the basalt fiber mix, in which super plasticising

FIGURE 5.2: During casting of the polymer fiber mix, a plug formed in the pump.

admixture was added, due to the waiting time when the plug arose during casting of the polymer fiber mix.

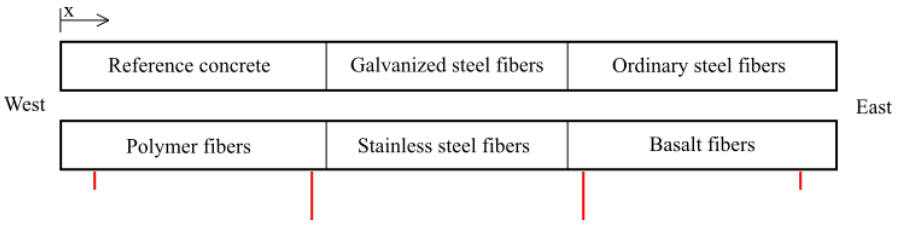

FIGURE 5.3: Simplified sketch of the location of the parts cast with different concrete mixes, from northwest to southeast. The red lines indicate the location of the columns.

According to Maage [1], there are some disadvantages with pumping:

- Stricter requirements to concrete composition
- Lubricating cement slurry or mortar has to be disposed outside the formwork
- Stricter demands for continuous placing
- Increased risk for breakdown of equipment, pipes etc vital to the placing-/production process
- Functional problem at pumping downhill
- Affects the concrete quality, for example the effect on air content
- Requirements for increased fines content increases the shrinkage potential of the concrete

All of the mixes were vibrated with a vibrator during placing of the concrete. When the forms were filled, the concrete was leveled out with a brick trowel. After trowelling, the concrete was sprayed with a membrane hardener called Pieri Curing Clear. This is applied to reduce desiccation of the surface, plastic shrinkage and the porosity of the concrete, as well as increasing the abrasion resistance of the concrete surface [12].

For each of the mixes, two cubes for compressive strength testing were cast. For each of the fiber mixes, three prisms were cast for testing of the residual tensile strength. The casting of this beams was done according to the procedure in NS-EN 14651, chapter 7 [13].

$NS - EN$ 14651, 7.1 gives that the geometry of the prisms shall be 150 mm $\times$ 150 mm $\times$ L, where 550 mm $\leq$ L $\leq$ 700 mm.

The procedure that was used for filling the prisms is according this standard, and is indicated in Figure 5.4. The order of filling is indicated by 1 and 2. The size of increment 1 should be twice the size of increment 2. The mould should be filled up to 90 % of its height before compaction by external vibration starts. During compaction the form shall be topped up and leveled off.

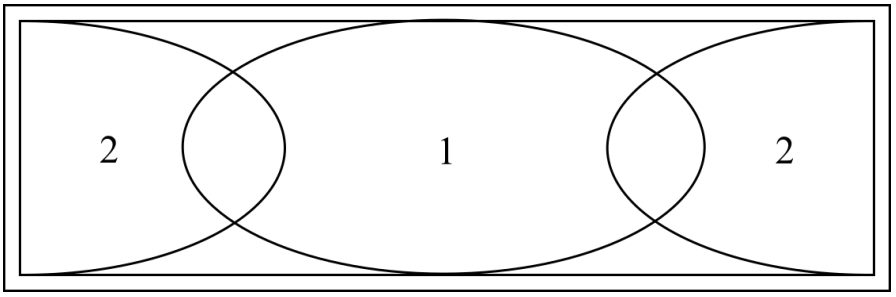

FIGURE 5.4: Filling procedure of test prisms. Illustration adapted from NS-EN 14651, chapter 7.1 [13].

May 9, it was performed an inspection and an accurate crack mapping of the edge beams. The interface between the different mixes was done well, but the concrete surface was a bit rough. The steel fibers and the galvanized steel fibers that protrude from the surface were corroded, but there was not observed any rust in the concrete surface. The polymer fiber mix which contained $8kg/m^3$ fibers had a bad looking surface, which was expected due to its dryness and stiffness during casting. All crack widths were measured, and the results are listed in Table 5.3, which also contain comments. The average crack widths for each beam are calculated, and presented in Table 5.2. The results are later compared to the calculated values and included in the discussion.

TABLE 5.2: Average crack widths for the observed cracks in the different edge beams at Sandsgård Bridge.

Concrete mix	Average crack width
Reference mix	0.09
Galvanized steel fiber	0.08
Ordinary steel fiber	0.05
Basalt fiber	0.02
Stainless steel fiber	0.05
Polymer fiber	0.03

TABLE 5.3: Measured crack widths for the observed cracks in the different edge beams at Sandsgård Bridge.

Concrete mix	Distance from end	Crack width [mm]	Comments
Reference mix	9 m	0.05	Through the lower half of the edge beam.
	12 m	0.10	Through the lower half of the edge beam.
	14 m	0.075	Through the entire edge beam, through the bolt for fastening of railings.
	15 m	0.12	Through the height of the edge beam.
	16 m	0.10	Through the entire edge beam except for the lower part. The crack goes through the bolt for fastening of railings.
Galvanized steel fiber	18 m	0.05	Through the bolt for fastening of railings.
	19 m	0.10	Through the lower half of the edge beam.
Steel fiber	36 m	0.05	Through the bolt for fastening of railings Through the entire edge beam except for the lower part.
Basalt fiber	38 m	0.02	2 cm to each side of formwork tie.
Stainless steel fiber	18 m	0.05-0.10	Through the entire edge beam, but not continuous.
	24 m	0.02	Through formwork tie.
	25 m	0.05	10 cm of the lower part.
Polymer fiber	11 m	0.02	5 cm on the upper side and 10 cm on the lower side of the formwork tie.
	12.5 m	0.025	15 cm on the upper side of the formwork tie and all the way down to the end.
	13.5 m	0.05	Through the entire edge beam. Not continuous.
	14 m	0.02	5 cm to both sides of the formwork tie.
	14.3 m	0.025	5 cm on the upper side and 15 cm on the lower side of the formwork tie.
	15.8 m	0.05	5 cm on the upper side and 15 cm on the lower side of the formwork tie.
	16.2 m	0.05	5 cm to both sides of the formwork tie.

5.1.1 Comments

As this experiment showed, pumping of fiber concrete may give rise to problems. To increase the pumpability of the mixes, the constituent of fines should be increased. It is important to note that one should not necessarily add more cement, due to the risk of increase in plastic shrinkage. One should rather add more sand and fine aggregates. This way plugs might be avoided. However, this was not chosen to do in this experiment, because a direct comparison with the reference beam was desirable.

5.2 Residual Flexural Tensile Strength

The residual flexural tensile strength, $f_{R,i}$ for the fiber mixes were obtained by performing a three point flexural test in the laboratory. During the test, the loads were plotted against the deflection of the test prisms. According to *Utkast til norsk betongforenings publikasjon nr 38*

[14], the basis for the calculation is the load at the first crack, as well as four predetermined crack widths: 0.5 mm, 1.5 mm, 2.5 mm and 3.5 mm. The calculated average residual flexural tensile strength for the fiber mixes used at Sandsgård Bridge, are plotted in Figure 5.5. Finally, the residual tensile strength representative for the service limit state, is calculated from the expression:

$$f_{fres} = 0.45 \times f_{R1} \tag{5.1}$$

where f_{R1} is the characteristic residual flexural tensile strength at a crack mouth opening displacement (CMOD) of 0.5 mm.

Figure 5.5 shows that the residual strength for the concrete with ordinary steel fibers differs a lot from the typical development of the residual strength for the other steel fibers. It is likely to think that this is due to that the concrete that was tested, was not representative for the whole mix. Most likely did this concrete portion contain more fibers than the rest of the mix, and gave hence too high values for the residual flexural tensile strength. It is therefore chosen to exclude this result from the calculation. For the three steel fiber mixes, the residual tensile flexural strength is calculated as the average value from the galvanized and stainless steel fiber mixes.

$f_{fres,steel} = 0.45 \times \frac{2.6+3.1}{2} = 1.28\ N/mm^2$

For the polymer fiber mix, the curve drops linearly in the first part. This indicates that this part is an unstable area of the graph, and that the computer hasn't been able to plot the measurements in this interval. Therefore it is chosen to use the first plotted value, that is $f_{R1} = 0.62\ N/mm^2$, for the polymer fiber mix. The residual strength is:

$f_{fres,polymer} = 0.45 \times 0.62 = 0.28\ N/mm^2$

For the basalt fiber mix, the residual strength is:

$f_{fres,basalt} = 0.45 \times 3.4 = 1.53\ N/mm^2$

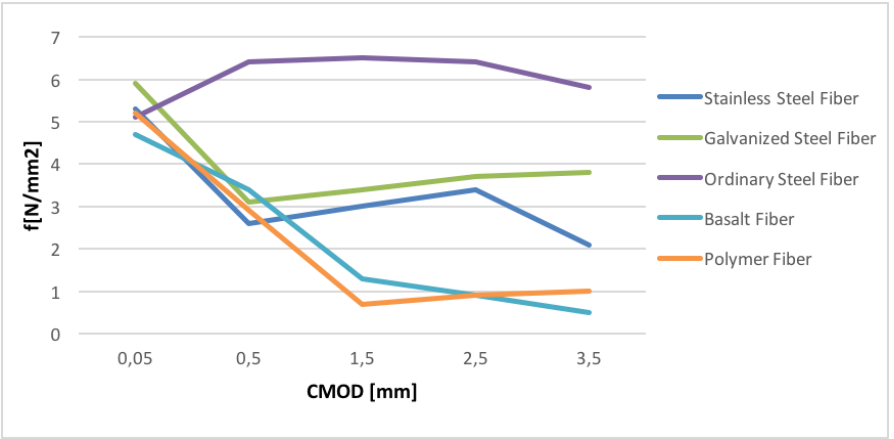

FIGURE 5.5: The residual tensile strength for the fiber beams at Sandsgård Bridge.

Further details about the residual flexural tensile strength for the prisms, are presented in Appendix B.

Chapter 6

CrackTeStCOIN

6.1 General

CrackTeStCOIN is a computer program based on the finite element method, that is used for modeling concrete structures. The program is adapted to Norwegian conditions and makes it possible to assess the risk of cracking in concrete due to imposed deformations at early ages. CrackTeStCOIN simulates the temperature and stress development in a structure, and based on this, the risk of cracking or the amount of cracking may be estimated. The impact of various measures to reduce or eliminate the risk of cracking can also be described [3].

6.2 Modeling the Laboratory Experiment

6.2.1 Simulation specifications

The formwork is modeled as wood/plywood 0.02 m with heat conductivity 0.14 W/Km, and in the program the styrofoam is modeled as "expanded polyethylene" 0.05 m, with heat conductivity 0.036 W/Km. Plywood and styrofoam are placed along the sidewalls. The bottom side of the slab and the top side of the edge beams are modeled with styrofoam. The top side of the slab is modelled as a free surface. The formwork and the styrofoam along the sidewalls and the top of the edge beams are removed after 72 hours. The simulation model is shown in Figure 6.1.

The simulation time is set to 600 hours. Both the ambient temperature and the start temperature for the concretes are set to 20 °C. The slab is modeled with Mature semi low-heat concrete, 20 % FA, while the edge beams are modeled with Semi low-heat concrete, 20 % FA. In both cases, the heat conductivity of the concrete is set to 2.1 W/mK. The restraint against lateral movement is set to 0, while restraint around the x- and y-axis is set to 1.

Heating cables were installed in the slab. These were turned on August 24, 8:30 am, which corresponds to 287 hours after casting. At this time the temperature in the edge beams had

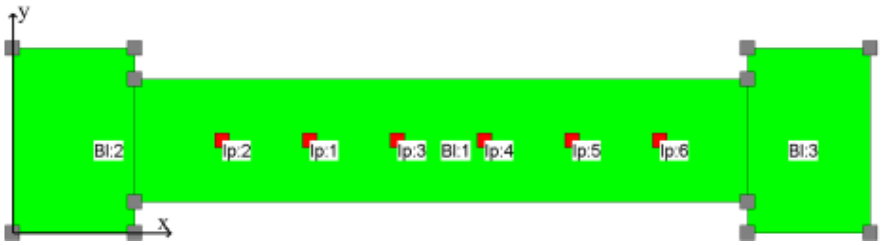

FIGURE 6.1: The simulation model of the laboratory experiment, modeled in CrackTeStCOIN.

dropped to the ambient temperature. The heating cables are modeled as six inner points, with equal distances, and the heating effect is modeled as 30 W/m. The cables were turned off after 72 hours, corresponding to 369 hours after casting of the edge beams.

6.2.2 Results

The largest tensile stresses are expected to occur in the edge beams, due to the temperature differences between the beams and the slab. The temperature development in the middle of the edge beam is plotted, and the result is shown in Figure 6.2.

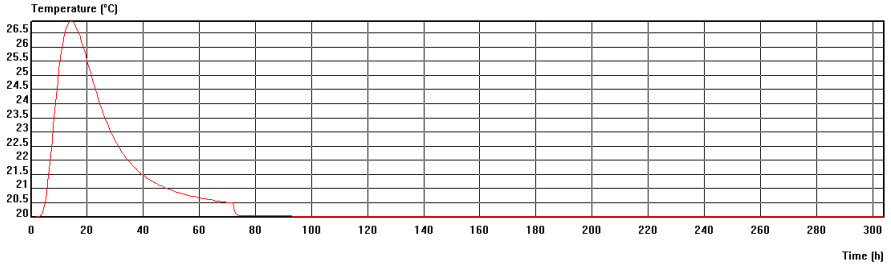

FIGURE 6.2: The temperature development in the middle of the edge beam as function of time.

From the temperature plot, it is seen that the maximum temperature occurs about 15 hours after casting. It is therefore interesting to look at the temperature and stress distribution after 15 hours. The temperature in the structure 15 hours after casting is shown in Figure 6.3.

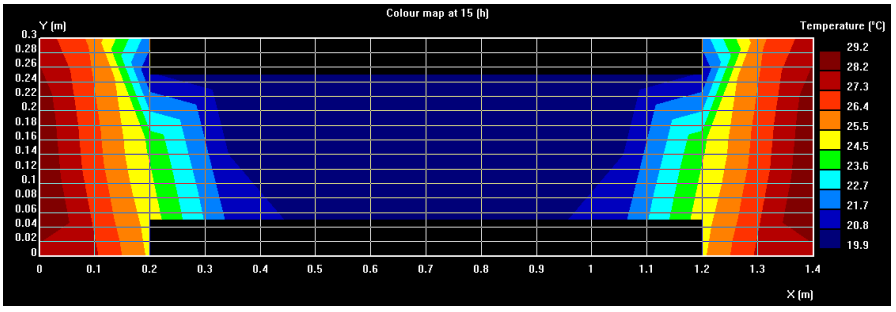

FIGURE 6.3: The simulated temperature in the structure 15 hours after casting.

The figure shows that the temperature reaches 29.2 °C in the edge beams 15 hours after casting. The maximum temperature in the middle of the slab is 19.9 °C at this point. The temperature

difference between the slab and the beams equals 9.3 °C. The resulting stresses are presented in Figure 6.4. The maximum tension stress of 0.195 MPa corresponds to a crack index of 0.187.

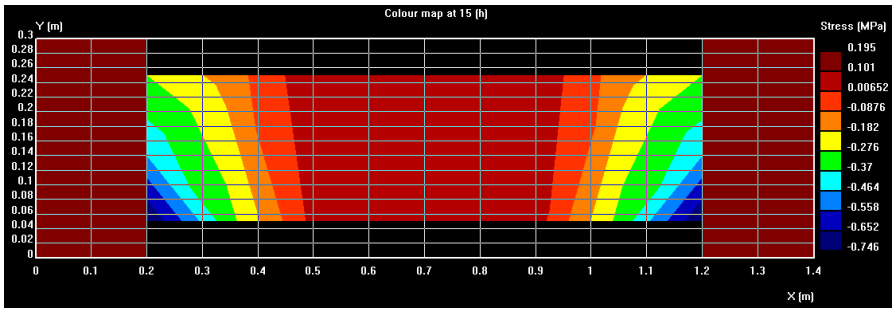

FIGURE 6.4: The simulated stresses in the structure, 15 hours after casting.

The crack index is defined as the ratio between the occurring stress and the tensile strength. If the crack index exceeds 1, cracks will form. To evaluate the risk of cracking, the occurring stresses must be checked against the tensile strength of the concrete at the given time. The tensile strength after 15 hours is calculated from Eurocode 2, 3.1.2 (9):

$$f_{ctm}(0.625d) = e^{0.25\times(1-\sqrt{28/0.625})} \times 3.8\text{MPa} = 0.915 \text{ MPa}.$$

This corresponds to a calculated crack index of 0.213. This indicates that no cracks are expected to occur at such an early stage in the hardening phase.

If one study the crack indices in the middle of the edge beam as a function of time, it is observed that the crack indices are largest a long time after casting, see Figure 6.5. Therefore, it is more likely that cracks will occur at the end of the curing period. However, the crack indices do only reach 0.5 before the heating cables are turned on, and hence it is not likely that the crack development has started at this point of time. This corresponds well with the fact that there was not observed any cracks during the curing phase in the laboratory. Cracking is expected to occur when the crack index exceeds 1, corresponding to the time span 300-385 hours after casting, that is; during heating of the slab.

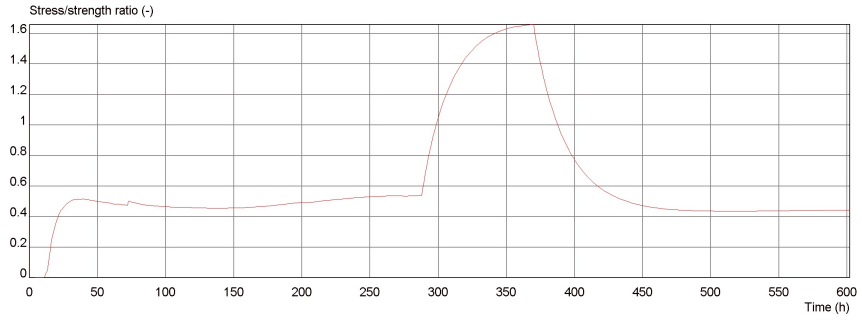

FIGURE 6.5: The development of the crack indices in the edge beams in the laboratory experiment, described as a function of time.

As mentioned previously, the heating cables in the slab was turned on 287 hours after casting the edge beams. They were turned off after 72 hours, corresponding to 369 hours after casting of the edge beams. Hence, it is interesting to study the temperature and stress distribution 369

hours after casting. The measured temperature in the slab was then 70.4 °C. This corresponds well with the simulated temperature distribution, shown in Figure 6.6, where the maximum temperature reaches 71.3 °C.

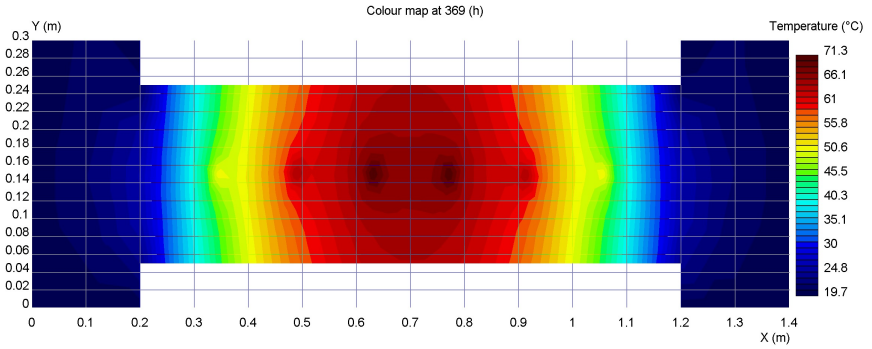

FIGURE 6.6: The temperature distribution in the structure right after the heating cables were turned off, 369 hours after casting. The simulated maximum temperature equals 71.3 °C.

The maximum temperature stresses occur when the temperature difference between the slab and the edge beams is at its maximum. The maximum stresses are hence found right after the heating cables are turned off, 369 hours after casting. The stress distribution is plotted in Figure 6.7. The maximum stress occurs in the outer part of the edge beam and equals 5.0 MPa. This is a much higher tensile stress than the tensile strength of the concrete, and hence it is expected that cracking has occurred at this moment.

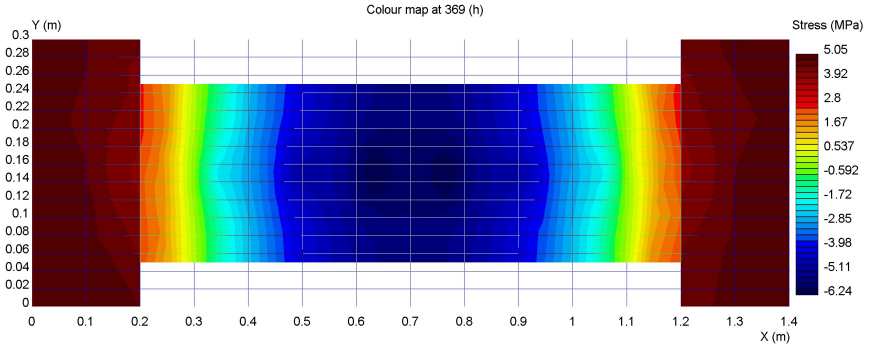

FIGURE 6.7: The stress distribution in the structure right after the heating cables were turned off, 369 hours after casting. The maximum stress occurs in the outer part of the edge beams and equals 5 MPa.

The tensile strength of the concrete is calculated from Eurocode 2, 3.1.2 (9):

$$f_{ctm}(15) = e^{0.25\times(1-\sqrt{28/15})} \times 3.8\text{MPa} = 3.47 \text{ MPa}$$

Due to this, it is clear that cracks are expected to occur at this point of time, according to the simulation. To estimate when the first crack is likely to occur, the stress development over time for the outer part of the edge beam is illustrated in Figure 6.8. The development of the tensile strength of the concrete is plotted together with the stress development in Figure 6.9. The first crack is expected to occur when the concrete stress reaches the strength. According to Figure 6.9 this happens after 322 hours. This corresponds to 35 hours after the heating cables were turned on. In the laboratory experiment, the first cracks were observed 6 hours after the heating

cables were turned on. Hence is the simulated stresses from CrackTeStCOIN, most likely too low.

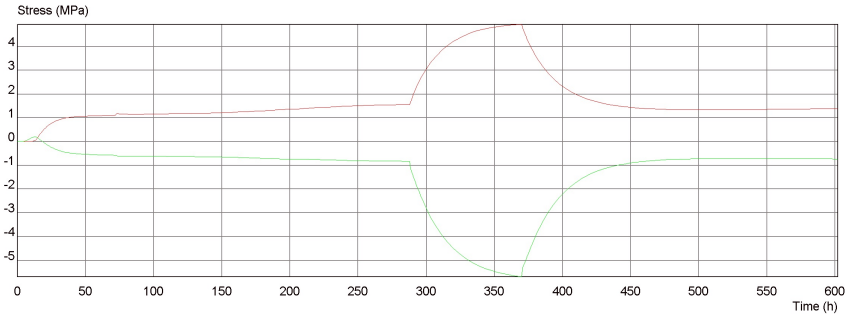

FIGURE 6.8: The simulated stress development as a function of time. The red graph shows the stresses in the outer part of the edge beam, while the blue graph illustrates the stresses in the middle of the slab.

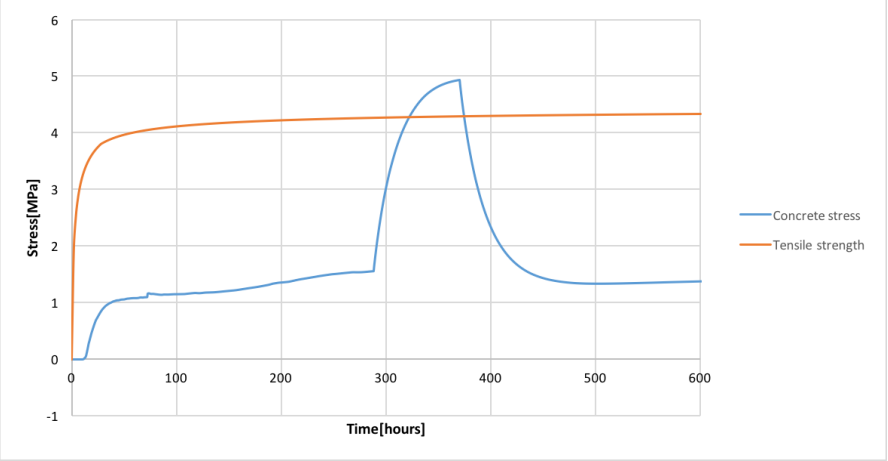

FIGURE 6.9: The simulated stress development in the edge beam, plotted together with the tensile strength development.

6.2.3 Comment

As a simplification, the ambient temperature in the laboratory experiment is modeled as constant equal 20 °C. This does not correspond with the actual case. The daily temperature inside the laboratory is expected to follow the outside temperature to some extent, which should give a contribution to stresses. Anyway, the stresses in the curing phase were so low that it is reasonable to think that no cracks were formed, even if this contribution was added. It was the temperature stresses from the heating phase that were the main part of the crack-inducing stresses. Compared to these, the contribution from the daily variation is so small that it is OK to disregard it.

6.3 Modeling Sandsgård Bridge

6.3.1 Simulation specifications

The Sandsgård Bridge was modelled with concrete *C40/50 Anlägg (Swe) w/c = 0.38 Air*. This concrete has a density of 2350kg/m^3 and a heat conductivity of 1.7 W/mK. The computation time was set to 1000 hours. The start temperature differs for each of the edge beams. The start temperature for the reference beam is chosen in the simulation. This equals 12.9 °C.

Based on the ambient temperatures in Sandnes during the period prior to casting, the start temperature for the deck was modeled as 5 °C. The start time for the plotted ambient temperatures are set to the day before casting, March 16, at midnight.

6.3.2 Results

There were not installed any temperature sensors in the bridge deck during this large scale experiment, and hence there exist no information about the temperature development in the deck. It is assumed that a good estimate for the temperature development is obtained by entering the real ambient temperatures in the program, and then plot the temperature development for the deck. To make sure that the temperature in the deck is following the ambient temperature when the casting of the edge beams is simulated, also the ambient temperatures from the day before casting are entered in the program. The temperatures are obtained from www.yr.no, logged at Sola weather station, located 7 km from Sandnes.

The ambient temperatures for the first 280 hours after casting were measured on the construction site. Figure 6.10 compares these values with the ones obtained from www.yr.no. The two graphs correspond well, with only a few large deviations. This justifies using values from www.yr.no as an estimate for the temperature development.

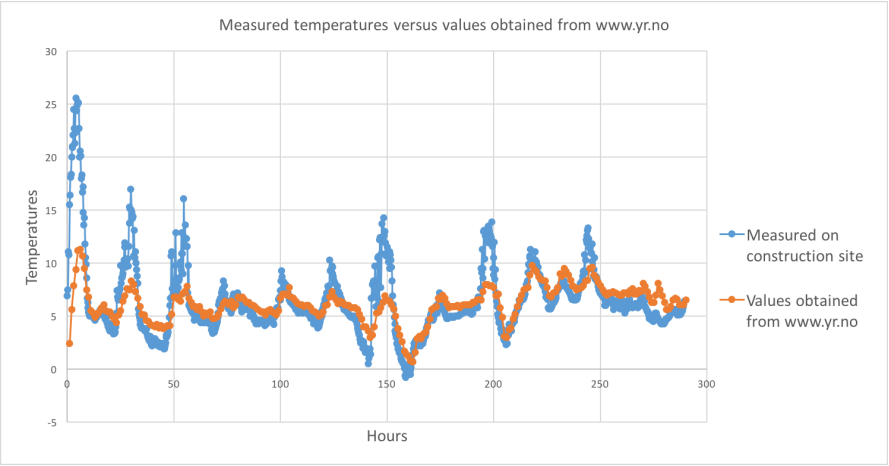

FIGURE 6.10: Measured temperatures plotted together with the values obtained from www.yr.no.

The temperature in the middle of the edge beam and the temperature in the middle of the deck are simulated, and the maximum temperature differences obtained are used to calculate

the resulting maximum stress in the early phase. Figure 6.11 illustrates the simulated case, while Figure 6.12 shows the measured temperatures in the edge beams plotted together with the simulated temperature in the deck.

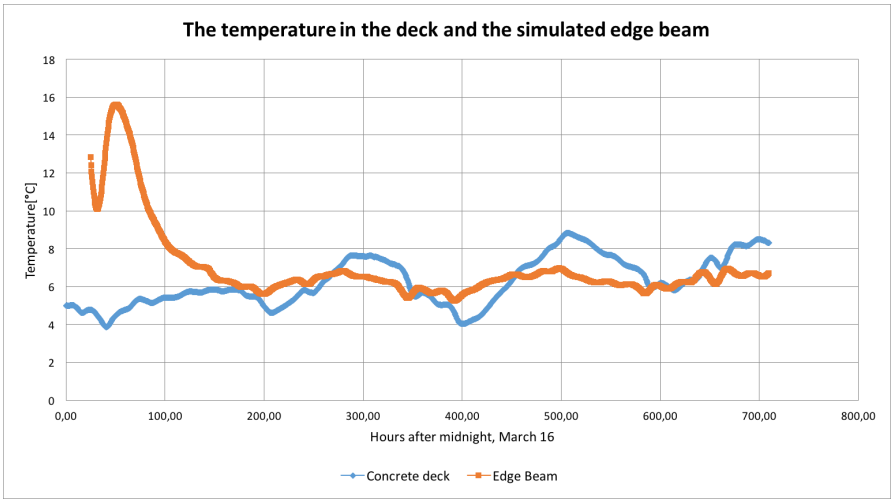

FIGURE 6.11: The simulated temperature in the deck plotted together with the simulated temperature in the edge beam.

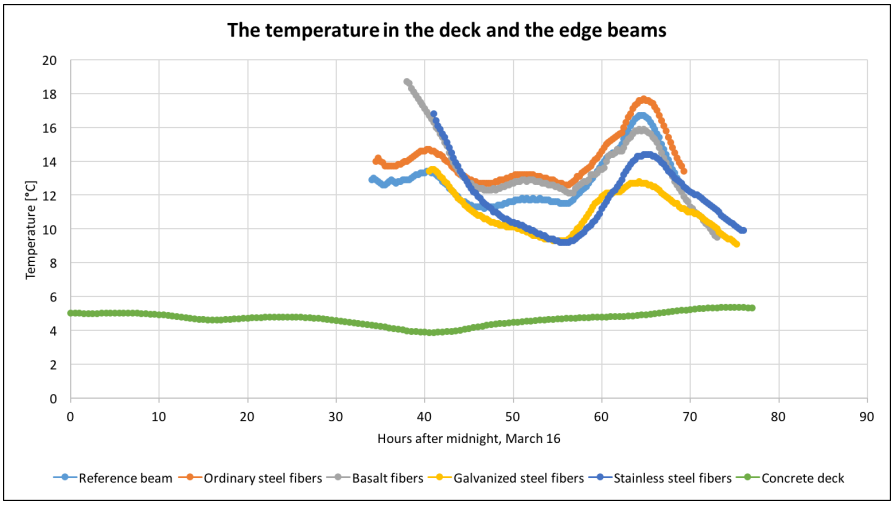

FIGURE 6.12: The simulated temperature in the deck plotted together with the measured temperatures in the different edge beams.

It was cast two curing boxes, one for the reference mix and one for the steel fiber mix. The temperature development for the curing boxes are presented in Appendix C.

As Figure 6.12 illustrates, the maximum temperature difference occurs for the ordinary steel fiber concrete, and the difference equals 12.8 °C. The maximum temperature difference in the simulated case equals 11.1 °C. Due to small deviations in temperature between the edge beams and the model in the analysed time interval, it is assumed that the model can be used to estimate the long term temperature development in the edge beam.

The maximum stress is expected to occur in the edge beam. The edge beam is small relative to the massive deck, and is hence more prone to a large degree of restraint, which in turn will lead to stresses. The temperature is decreasing towards the surface. It is therefore chosen to

study the temperature and stress development in the middle of the upper part of the edge beam. The point (0.28, 0.53) is chosen. The lower, left corner of the edge beam is placed in the origin. Figure 6.13 shows the simulated temperature development over time for the chosen point.

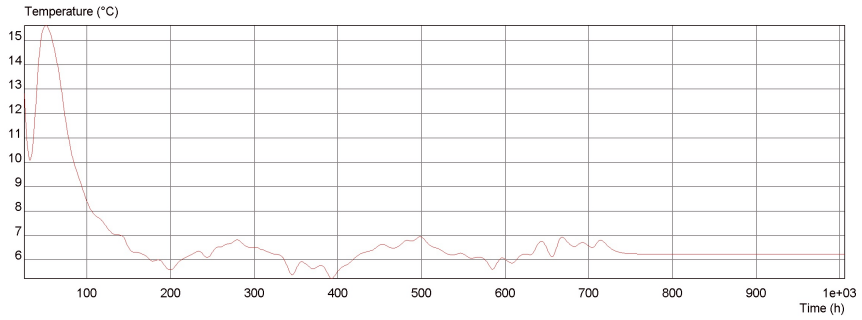

FIGURE 6.13: The simulated temperature development in the middle of the upper part of the edge beam, point (0.28,0.53).

The graph shows that the maximum temperature occurs about 50 hours after casting of the edge beams. Hence, it is chosen to study the stresses 50 hours after casting, plotted in Figure 6.14.

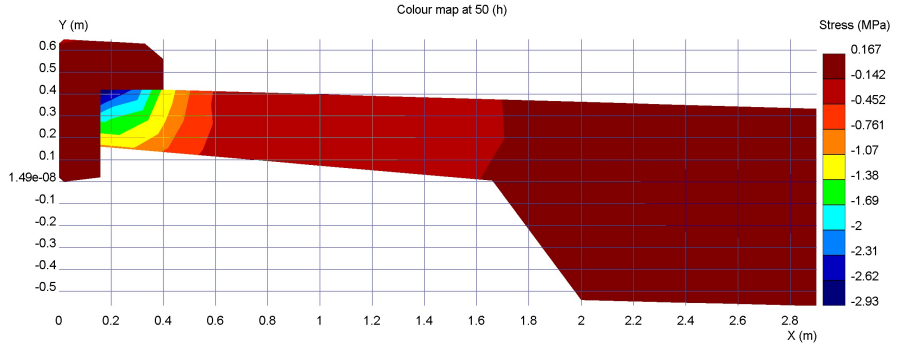

FIGURE 6.14: The stress distribution in Sandsgård Bridge, 50 hours after casting of the edge beams.

Figure 6.14 shows that the tensile stresses are low 50 hours after casting. This was expected since the edge beams are expanding during the hydration in the early age, hence this is the compressive phase for the edge beams. However, the figure shows that the maximum stresses occur in the upper part of the edge beam, and hence is the considered point (0.28, 0.53) a reasonable choice for the simulation. The stress development over time is plotted for this point, shown in Figure 6.15.

Figure 6.15 shows that the maximum tensile stress that occurs during the first 1000 hours after casting equals 1.75 MPa, and it occurs after approximately 200 hours.

It is also interesting to simulate the bridge deck with the concrete *Semi low-heat concrete, 20 % FA*. This concrete has a density of 2335 kg/m^3 and a heat conductivity of 3.7 W/Km. The simulated stress development is presented in Figure 6.16. The maximum stress reaches 0.7 MPa for this concrete.

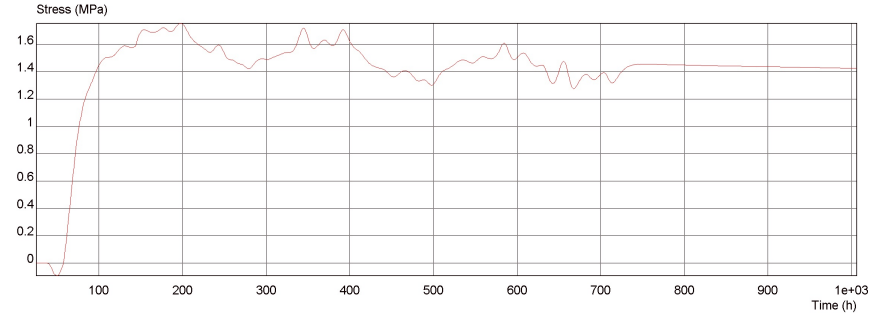

FIGURE 6.15: The stress development over time in the edge beam of Sandsgård Bridge.

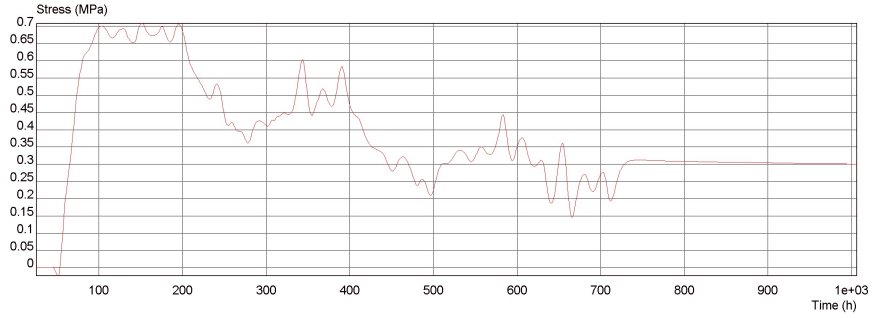

FIGURE 6.16: The stress development over time in the edge beam of Sandsgård Bridge.

The tensile strength after 8 days (200 hours) equals 3.06 MPa. Hence, the simulation in CrackTeStCOIN gives that no cracking should occur during the first 1000 hours. This, however is not corresponding with the observed cracks on the edge beams.

Chapter 7

Temperature Calculations - Sandsgård Bridge

7.1 Temperature Stresses

The temperatures in the middle of each edge beam on Sandsgård Bridge were plotted against time. The temperature development for each concrete mix and the ambient temperature during the first 300 hours are shown in Figure 7.1 and Figure 7.2. The temperature developed during hydration is one of the main reasons for volume changes in concrete. These volume changes can create stresses, which may lead to crack development. Cracks as a result of external restraint start to propagate during the cooling phase of the concrete [1]. In the simplified calculations of the temperature stresses in this thesis, therefore only the maximum temperature differences in the cooling phase are considered.

The Norwegian Public Roads Administration's *Prosesskode 2* formulates three temperature requirements, presented in Chapter 2.2 in this thesis. The fulfillment of these requirements is to be assessed for Sandsgård Bridge. It was only installed one temperature sensor in each concrete mix, which makes it impossible to check the temperature differential over the cross-section. Hence, it is not possible to check the second requirement, but due to the slenderness of the edge beams it is reasonable to think that this requirement is fulfilled.

Despite the fact that the temperature in the middle of a cross-section is higher than in the rest of the cross-section, the temperatures from the middle of the structure parts are used in the calculations. This is justifiable since it is a conservative choice, due to the fact that the calculated stresses then will be at its maximum. Also, the maximum stresses will be the crack inducing stresses. The two requirements that will be checked are illustrated in Figure 2.1.

The temperature development for each concrete mix and the ambient temperature during the first 72 hours are plotted in Figure 7.3 and 7.4. From these figures it is easily seen that the temperature never exceeds 65 °C in none of the concrete mixes, and hence is the first requirement fulfilled.

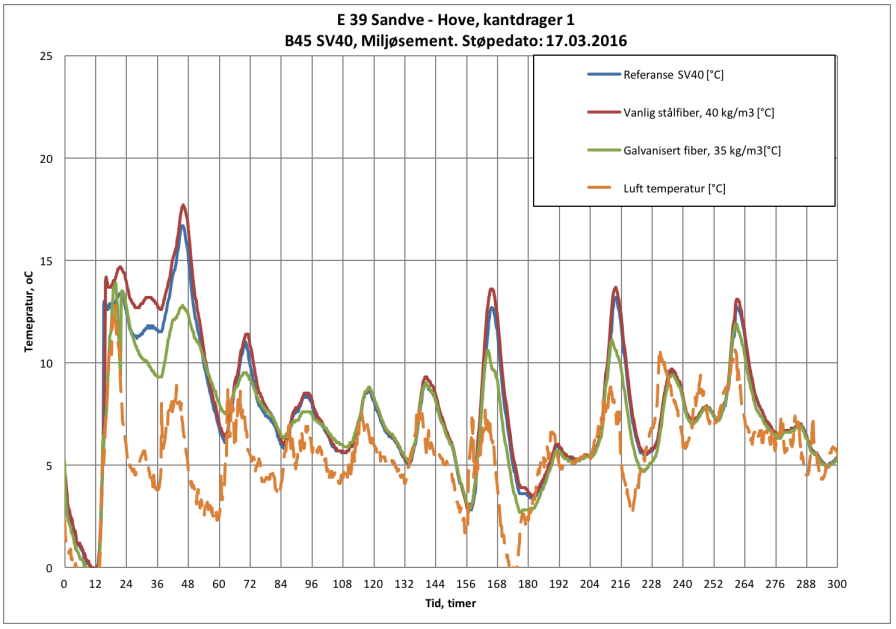

FIGURE 7.1: Temperature development during the first 300 hours after casting for the concrete mixes with steel fibers, galvanized steel fibers and the reference concrete, plotted together with the ambient temperature.

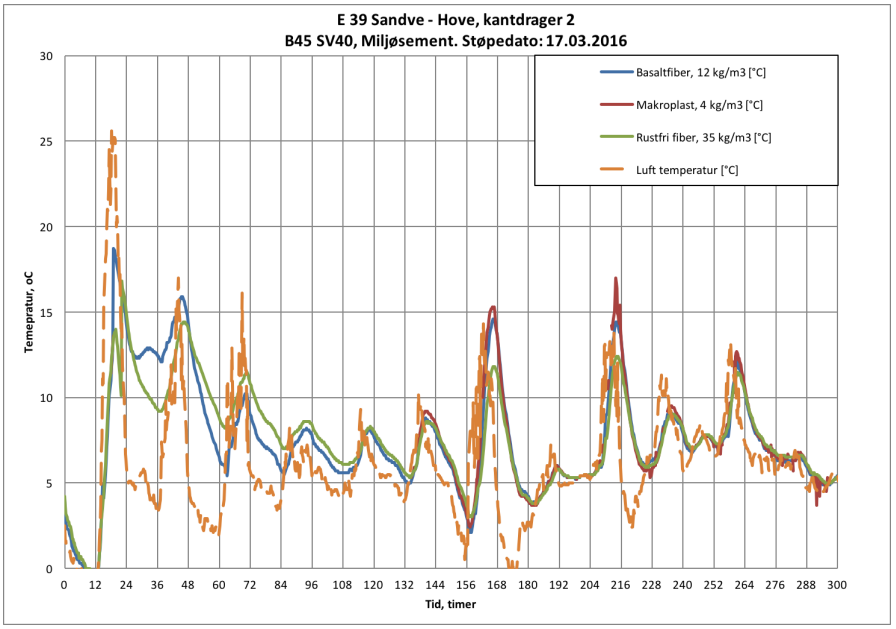

FIGURE 7.2: Temperature development during the first 300 hours after casting for the concrete mixes with basalt fibers, polymer fibers and stainless steel fibers, plotted together with the ambient temperature.

It is assumed that the temperature development for the bridge deck, simulated in Section 6.3, is valid. The temperature strain is calculated from the temperature difference between the edge beams and the bridge deck. The maximum temperature differences for each concrete mix is listed in Table 7.1.

As shown in Table 7.1, the maximum temperature difference occurs in the steel fiber mix. The difference equals 12.8 °C, and hence is also the last requirement fulfilled.

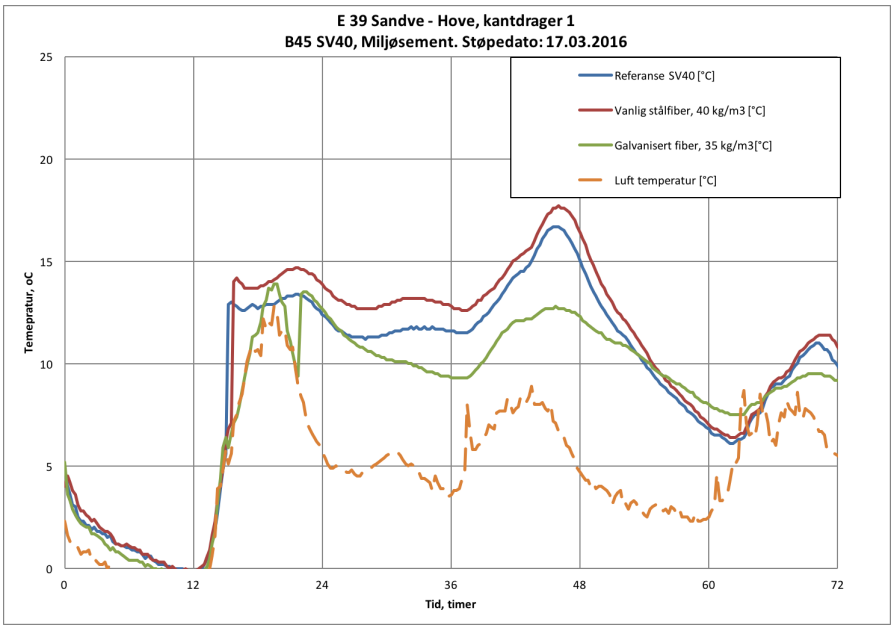

FIGURE 7.3: Temperature development during the first 72 hours after casting for the concrete mixes with steel fibers, galvanized steel fibers and the reference concrete, plotted together with the ambient temperature.

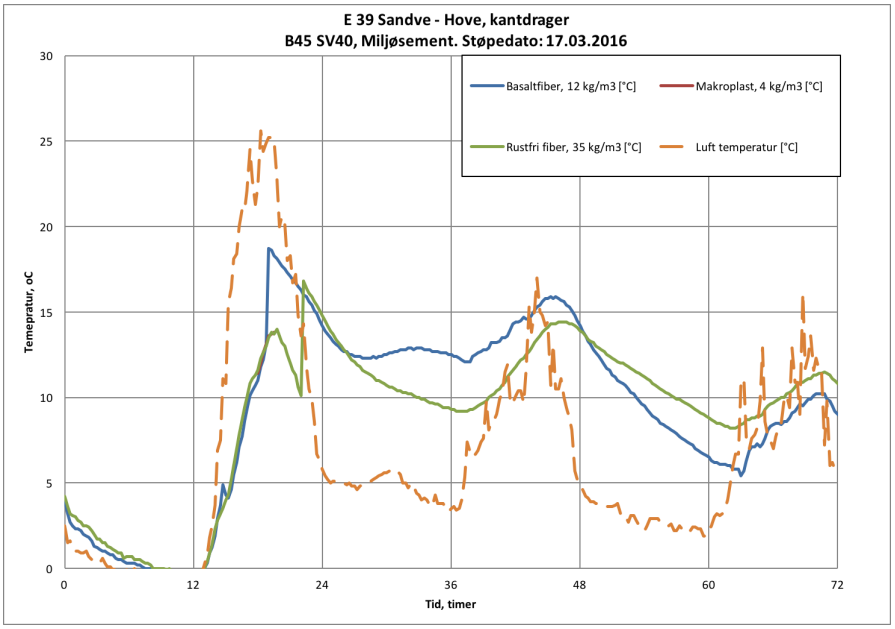

FIGURE 7.4: Temperature development during the first 72 hours after casting for the concrete mixes with basalt fibers, polymer fibers and stainless steel fibers, plotted together with the ambient temperature.

The concrete strain is calculated by the assumption that the coefficient of thermal expansion is $9 \times 10^{-6}/\text{C}^\circ$. The thermal strain is calculated from equation 2.1. The calculated values are shown in Table 7.2.

The stresses from the temperature strain is calculated from the formula:

TABLE 7.1: Maximum temperature differences between edge beams and the bridge deck.

Concrete mix	Maximum temperature difference [°C]
Reference concrete	11.8
Steel fibers	12.8
Galvanized steel fibers	7.8
Basalt fibers	11.0
Stainless steel fibers	9.5

TABLE 7.2: Calculated temperature strains in the different concrete mixes.

Concrete mix	Temperature strain [‰]
Reference concrete	0.106
Steel fibers	0.115
Galvanized steel fibers	0.070
Basalt fibers	0.099
Stainless steel fibers	0.086

$$\sigma_T = \varepsilon_T \times E_{eff} \tag{7.1}$$

The temperature stresses is calculated from the assumption that the Young's modulus for the concrete is 30 000 MPa [15], and the effective Youngs modulus is calculated for a concrete with a creep coefficient of 1.5. $E_{eff} = (30000)/(1 + 1.5) = 12000$ MPa . The calculated values are given in Table 7.3. For further details about the chosen creep coefficient, see Chapter 10.

TABLE 7.3: Calculated temperature stresses in the different concrete mixes.

Concrete mix	Temperature stress [MPa]
Reference concrete	1.27
Steel fibers	1.38
Galvanized steel fibers	0.84
Basalt fibers	1.19
Stainless steel fibers	1.03

Additionally, the daily variation in temperature will lead to increased stresses in the concrete. According to www.yr.no, it is approximately a difference of 6 °C between the temperatures at night and at day, 6 weeks after casting. Since the edge beams are slender, they will follow the daily temperature variation to a greater extent than the bridge deck. It is assumed that the temperature difference between the bridge deck and the edge beams is equals approximately 3 °C. This equals a concrete stress of about

$\sigma_T = 3°C \times 9 \times 10^{-6}/°C \times 30000$ MPa $= 0.81$ MPa

7.2 Autogenous Shrinkage

The bridge deck was cast 04.03.16 and the edge beams were cast 17.03.16. The maximum temperature difference between the deck and the slab occurs about 30 - 35 hours after casting of the beams. At this time the age of the bridge deck is about 14.5 days and the age of the beams is about 1.5 days.

This gives a difference in autogenous shrinkage strain of:

$$\Delta\varepsilon_{ca} = \varepsilon_{ca}(1.5) - (\varepsilon_{ca}(14.5) - \varepsilon_{ca}(13.5)) =$$
$$((1 - e^{-0.2\times1.5^{0.5}}) - ((1 - e^{-0.2\times14.5^{0.5}}) - (1 - e^{-0.2\times13.5^{0.5}}))) \times 2.5(45 - 10) \times 10^{-6} = 0.0179‰$$

As for Section 7.1, also here an effective Youngs modulus of 12 000 MPa is used. This corresponds to a concrete stress of:

$$\Delta\sigma_{ca} = \Delta\varepsilon_{ca} \times E_c = 0.0179‰ \times 12000 \text{ MPa} = 0.21 \text{ MPa}$$

7.3 Total Concrete Stress

The total concrete stress is obtained by superposing the three contributions calculated above. The largest temperature difference occurred in the steel fiber mix, and it is therefore chosen to calculated the total stress in this mix.

$\sigma_{\text{c,steelfiber}} = 1.27$ MPa $+0.81$ MPa $+0.21$ MPa $= 2.29$ MPa

The calculated stress is less than the tensile strain capacity, and hence cracks are not expected to occur according to these calculations.

The stress corresponds to a tensile strain of 0.19 ‰.

Chapter 8

Calculation of Crack Widths due to Shrinkage Cracking in Fully Restrained Members

In this section, the calculations are performed according to ACI Structural Journal, vol.89 no.2 [11], presented in Section 3.2.

One of the edge beams that were cast in the laboratory is considered. The beam is 1000 mm long, 300 mm high and 200 mm thick. It is a reinforced concrete beam, which is restrained along one edge. The beam contains 8 mm diameter longitudinal bars placed 55 mm from the outer edge of the beam. Both the top and bottom concrete cover to the reinforcement is 40 mm. Two reinforcement bars are placed between the top and the bottom reinforcement, in a distance of 55 mm from the outer bars.

The steel area is $A_s = 4 \times \pi \times 4^2 \times = 201.1$ mm^2.

Assumptions made in the calculations:

- $E_c = 30\ 000$ MPa
- $E_s = 200\ 000$ MPa
- $f_y = 500$ MPa

The temperature difference between the slab and the beam is at its maximum right after the heating cables are turned off. The age of the slab is then 64 days, while the age of the edge beam is 15 days. Mathematical formulas for the autogenous shrinkage are formulated in Eurocode 2, 3.1.4 (6) [8]:

$$\varepsilon_{ca}(t) = \beta_{as}(t)\varepsilon_{ca}(\infty) = (1 - \mathrm{e}^{-0.2t^{0.5}}) \times 2.5(f_{ck} - 10) \times 10^{-6} \tag{8.1}$$

where t is the age of the concrete, given in days.

The characteristic compressive strength is obtained from Eurocode 2, Table 3.1, and is set equal to 45 MPa. This gives

$\varepsilon(\infty) = 2.5 \times (45 - 10) \times 10^{-6} = 0.0875‰$

The autogenous shrinkage strain in the slab is calculated after both 64 days and 49 days:

$\varepsilon_{ca}(64) = \beta_{as}(64)\varepsilon_{ca}(\infty) = (1 - e^{-0.2 \times 64^{0.5}}) \times 8.75 \times 10^{-5} = 0.0698‰$

$\varepsilon_{ca}(49) = \beta_{as}(49)\varepsilon_{ca}(\infty) = (1 - e^{-0.2 \times 49^{0.5}}) \times 8.75 \times 10^{-5} = 0.0659‰$

The autogenous shrinkage strain in the edge beam is then calculated: $\varepsilon_{ca}(15) = \beta_{as}(15)\varepsilon_{ca}(\infty) = (1 - e^{-0.2 \times 15^{0.5}}) \times 8.75 \times 10^{-5} = 0.0472‰$

The difference between the strain in the slab after 64 days and 49 days is subtracted from the strain in the edge beam. This is the stress-inducing strain, and the difference equals:

$\Delta\varepsilon_{ca} = 0.0472‰ - (0.0698‰ - 0.0659) = 0.0433‰$

The temperature difference between the slab and the beam is also leading to stresses. In the calculation of the temperature strain, the thermal expansion coefficient is set to $\alpha_T = 9 \times 10^{-6}$, based on experience from NTNU [16].

The temperature strain is given by

$\Delta\varepsilon_T = \alpha_T \times \Delta T,$

where ΔT is the temperature difference between the two considered sections.

The following information is obtain from the specialization project:

- The maximum temperature difference between the slab and the edge beam during heating of the slab, was equal to 34 °C. This equals a strain difference of 0.30 ‰.
- The maximum temperature difference between the slab and the edge beam during hydration of the edge beams was equal to 16 °C. This equals a strain difference of 0.14 ‰.

The drying shrinkage develops slowly, and is hence not included in the calculations in this case.

It is assumed that the strain contribution from the hardening phase still applies in the heating phase. Therefore, the sum of the above-mentioned strains is used when calculating the resulting strain.

$\Delta\varepsilon = 0.30‰ + 0.14‰ + 0.0433‰ = 0.48‰$

The creep coefficient is obtained from Eurocode 2, 3.1.4(5), Figure 3.1(a). t_0 is the age of the concrete at time of loading in days, in this case 15 days. h_0 is the notional size $= 2 \times A_c/u$, where A_c is the concrete cross-sectional area and u is the perimeter of that part which is exposed to drying.

This gives:

$h_0 = \frac{2A_c}{u} = \frac{2\times200\times300}{2\times200+300+1000} = 150$ mm

The creep coefficient is found by using the method described in Eurocode 2, valid for C45/55 and concrete class N. Reading from Figure 3.1(a), this gives a creep coefficient equal to 2.

The tensile strength of the concrete is calculated from Eurocode 2, 3.1.2 (9) [8]. Assuming normal concrete and a characteristic compressive strength of $f_{ck} = 45$ MPa, the tensile strength after 15 days equals 3.47 MPa. $\rightarrow f_t = 3.47$ MPa

$n = E_s/E_c = 200000/30000 = 6.67$

The concrete area and reinforcement ratio can now be calculated:

$A_c = 300 \times 200 = 60000\ mm^2/m$

$\rho = \frac{A_s}{A_c} = \frac{201.1}{60000} = 0.0034$

From Equation 3.5:

$s_0 = d_b/(10\rho) = 8/(10 \times 0.0034) = 238$ mm

The final effective modulus is obtained from Equation 3.25:

$E_e^* = 30000/(1 + 2) = 10000$ MPa

and the corresponding effective modular ratio is:

$n^* = E_s/E_e^* = 200000/10000 = 20.$

Equation 3.10 gives:

$C_1 = (2 \times 238)/(3 \times 1000 - 2 \times 238) = 0.19$

and from Equation 3.16, the restraining force immediately after the first cracking is:

$N_{cr} = \frac{6.67\times0.0034\times3.47\times60000}{0.19+6.67\times0.0034(1+0.19)} = 21759.5$ N/m

From Equation 3.13 the concrete stress can be calculated:

$\sigma_{c1} = (21759.5(1 + 0.19))/60000 = 0.43$ MPa

An approximation of the average concrete stress is obtained from Equation 3.23:

$\sigma_{av} = (0.49 + 3.47)/2 = 1.95$ MPa

Equation 3.32 gives:

$\xi = \frac{-20\times0.0034(1.95+(-0.48\times10^{-3}\times10000))}{20\times0.0034(1.95+(-0.48\times10^{-3})\times10000)+3.47} = 0.059$

Equation 3.31 gives that the crack spacing must satisfy:

$s \leqslant (2 \times 238(1 + 0.059))/(3 \times 0.059) = 2840.9$ mm

The minimum number of cracks is $m \geqslant L/s = 1000/2840,9 = 0.35$.

Therefor $m = 1 \rightarrow s = \frac{L}{m}\frac{1000}{1} = 1000$.

From Equation 3.20 C_2 is calculated:

$C_2 = \frac{2\times238}{3\times1000-2\times238} = 0.19$

The final restraining force is calculated from Equation 3.29:

$N(\infty) = -(20 \times 201.1(1.95 + (-0.48 \times 10^{-3}) \times 10000))/0.19 = 60330$ N/m

The steel and concrete stresses are calculated from Equation 3.19, 3.21 and 3.26:

$\sigma^*_{s2} = 60330/201.1 = 300$ MPa

$\sigma^*_{s1} = -0.19 \times 300 = -57$ MPa

$\sigma^*_{c1} = (60330 + 57 \times 201.1)/60000 = 1.19$ MPa

The final crack width is determined by using Equation 3.34:

$w = -\left[\frac{1.19}{10000}(1000 - \frac{2}{3} \times 238) + (-0.48 \times 10^{-3}) \times 1000)\right] = 0.38mm$

Chapter 9

Early-age Thermal Crack Control - Calculation of Crack Widths

The calculations performed in this section are done in accordance with the British guideline *Early-age thermal crack control in concrete - CIRIA C660* [9]. The calculation method is performed both for the laboratory experiment and Sandsgård Bridge.

The allowable crack width is determined from the requirement of a durable concrete structure. The limiting total crack width arising from early-age deformations, long-term deformations and loading, is 0.3 mm. The full crack pattern is expected to occur at early age under conditions of edge restraint.

9.1 Laboratory Experiment

It is recommended to use a ratio of $E_0/E_n = 0.7-0.8$ in the early age. A ratio of 0.75 is therefore chosen. This gives the restraint for the early thermal cycle, calculated from Equation 3.39:

$R_1 = 1/\left(1 + \frac{200\times300\times0.75}{200\times1000}\right) = 0.82$

For the current case, assuming equal modulus of elasticity for the two pours, the restraint for medium- and long term deformation at the joint is:

$R_2 = 1/\left(1 + \frac{200\times300}{200\times1000}\right) = 0.77$

Since R_2 reflects the restraint after long time, it is assumed that the restraint factor for the drying shrinkage is equal. Hence $R_3 = R_2 = 0.77$.

T_1 is the difference between the peak temperature, T_p, and the mean ambient temperature, T_a, at the end of the thermal cycle. Values for T_1 for CEM II for walls cooling from both faces are given in Figure 9.1. The British guideline presents a table where the total binder content is given for different strength classes, *Table 4.2.* For a concrete in strength class C45/50 valid for

up to 20 % fly ash, the total binder content is 470kg/m^3. From Figure 9.1, valid for plywood formwork , 20 % fly ash, binder content $470kg/m^3$ and thickness $200mm$, $T_1 = 23°C$.

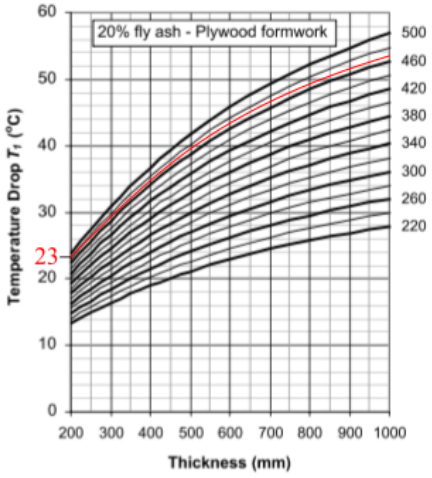

FIGURE 9.1: Values for T_1 for concrete with 20 % FA and plywood formwork.

T_2 is the difference between the mean ambient temperature at the end of the early thermal cycle and the minimum element temperature likely in the course of the element life. For annual temperature changes recommended values of T_2 are 20 °C for concrete cast in the summer and 10 °C for concrete cast in the winter. Hence, T_2 is set equal to 20 °C.

$K_{c1} = 0.65$ and $K_{c2} = 0.5$.

The autogenous shrinkage is obtained from *Table 4.5*, presented in the British guideline: $\varepsilon_{ca}(3) = 26 \times 10^{-6}$ and $\varepsilon_{ca}(28) = 57 \times 10^{-6}$.

The drying shrinkage is calculated from Eurocode 2, 3.1.4 (6): $\varepsilon_{cd}(t) = \beta_{ds}(t, t_s) \times k_h \times \varepsilon_{cd.0}$

Since the experiment was performed during summertime, it is assumed that the relative humidity is a bit high. It is therefore chosen to use RH = 60%. Interpolation gives a nominal unrestrained drying shrinkage, $\varepsilon_{cd.0}$, of 0.36 ‰.

$\beta_{ds}(t, t_s) = (t - t_s)/((t - t_s) + 0.04 \times \sqrt{h_0^3})$

t_s is the age of the concrete in days at the beginning of drying. This is normally at the end of the curing period, and t_s is hence set to 5 days. t is the age of the concrete at the given time, and is for the current case set to 15 days.

$h_0 = (2 \times A_c)/u = (2 \times 200 \times 300)/(2 \times 200 + 300) = 171.4$ mm

This gives:

$\beta_{ds}(15.5) = (15 - 5)/((15 - 5) + 0.04 \times \sqrt{171.4^3}) = 0.10$

Interpolation of the values from *Table 3.3* in Eurocode 2 gives an estimation of k_h:

$k_h = 1 - 0.15 \times 0.71 = 0.89$

The drying shrinkage can now be calculated:
$\varepsilon_{cd}(15) = 0.10 \times 0.89 \times 0.36$ ‰= 0.032 ‰

The tensile strain capacity is calculated from Equation 3.41:

$f_{ctm}(3) = e^{s[1-\sqrt{\frac{28}{3}}]} \times f_{ctm} = e^{0.25[1-\sqrt{\frac{28}{3}}]} \times 3.8 = 2.27$MPa

$E_{cm}(3) = (\frac{f_{cm}(3)}{f_{cm}})^{0.3} E_{cm} = (\frac{2.27}{3.8})^{0.3} \times 36 = 30.8$ GPa

Hence: $\varepsilon_{ctu}(ea) = 1.08 \frac{2.27}{30.8 \times 10^3} = 0.080$ ‰

The crack-inducing strain can now be calculated:
$\varepsilon_{cr} = 0.65[9 \times 10^{-6} \times 23 + 26 \times 10^{-6}]0.82 + 0.5[31 \times 10^{-6} \times 0.77 + 9 \times 10^{-6} \times 20 \times 0.77 + 0.032 \times 10^{-3} \times 0.77] - 0.5 \times 0.08 \times 10^{-3} = 0.217$ ‰−0.04‰= 0.177 ‰

The crack width is calculated from Equation 3.43:

$w_k = \varepsilon_{cr}(3.4c + 0.425 \frac{k_1 k_2 \phi}{\rho_{p,eff}}) = 0.177 \times 10^{-3} \times (3.4 \times 40 + 0.425 \times \frac{0.8 \times 1 \times 8}{0.01}) = 0.073$ mm

9.1.1 Comment

The temperature drop, T_1, is estimated under the assumption that the structure is a wall cooling from both faces. This is not a valid assumption for the current structure. It is bond between the edge beams and the bridge deck. T_1 is the difference between the peak temperature and the mean ambient temperature. The laboratory experiment was performed in indoor climate, and hence it is reasonable to believe that the mean ambient temperature was a bit higher than the basis for the curves presented in the British guideline. In that case, T_1 will be less, and the final concrete strain will be slightly lower than calculated.

9.2 Sandsgård Bridge

The edge beams are quite small relative to the bridge deck, and hence the restraint factors are set to 1 for the current case.

As previosly mentioned, T_1 is the difference between the peak temperature, T_p, and the mean ambient temperature, T_a, at the end of the thermal cycle. The British guideline presents different graphs for deducing values for T_1. These, however, are only valid for either walls cooling from both faces or ground slabs. It is therefore chosen to calculate T_1 from the temperature development that were measured at the construction site and the ambient temperatures obtained from www.yr.no, presented in Section 7.1. For the reference beam, the peak temperature equals 16.70 °C, while the mean ambient temperature equals 7.5 °C.

$T_1 = 16.70 - 7.5 = 9.2$ °C.

As for the calculation of the laboratory experiment, T_2 is set equal to 20 °C also here. $K_{c1} = 0.65$ and $K_{c2} = 0.5$. In both cases the strength class is C45/55, and hence is the autogenous shrinkage the same for both cases. $\varepsilon_{ca}(3) = 26 \times 10^{-6}$ and $\varepsilon_{ca}(28) = 57 \times 10^{-6}$.

The drying shrinkage is calculated from Eurocode 2, 3.1.4 (6). The concrete is cast outside, and hence is the relative humidity set to 80 %. Interpolation of the values in Eurocode 2, Table 3.2, gives an unrestrained drying shrinkage of 0.23% for $f_{ck} = 45$ MPa. t_s is set to 5 days and t is set to 52 days, since the crack mapping was performed 52 days after casting.

$h_0 = (2 \times A_c)/u = (2 \times 150450)/4292.9 = 70.1\text{mm}$

This gives: $\beta_{ds}(52.5) = (52-5)/((52-5) + 0.04 \times \sqrt{70.1^3}) = 0.67$

Interpolation of the values from Eurocode 2, Table 3.3, gives an estimation of k_h:

$k_h = 1 + 1.5 \times 10^{-3} \times 29.9 = 1.04$

The drying shrinkage can now be calculated:
$\varepsilon_{cd}(52) = 0.67 \times 1.04 \times 0.23$ ‰= 0.16 ‰

The calculation of the concrete area, $A_c = 150450$ mm^2, is presented in *Appendix A.2.*

The tensile strain capacity is the same for both cases, since it only depends on the concrete strength class. $\varepsilon_{ctu}(ea) = 0.080$ ‰

The crack-inducing strain can now be calculated:
$\varepsilon_{cr} = 0.65[9\times10^{-6}\times9.2+26\times10^{-6}]+0.5[31\times10^{-6}+9\times10^{-6}\times20+0.16\times10^{-3}]-0.5\times0.08\times10^{-3} =$ 0.22 ‰

$\rho_{p,eff} = A_s/A_{c,eff}$, where $A_{c,eff}$ is the effective area of concrete in tension surrounding the reinforcement of depth, $h_{c,ef}$. This is illustrated for the edge beams at Sandsgård Bridge in Figure 9.2. The reinforcement has a concrete cover of 65 mm, and hence is the effective thickness set to $h_{ef.1} = (65+16/2)\times2 = 146$ mm for the part with Ø16 rebars and $h_{ef.2} = (65+20/2)\times2 = 150$ mm for the part with Ø20 rebars. This gives an effective concrete area of:

$A_{ef} = 650 \times 146 + 254 \times 150 = 133000\text{mm}^2$

In the calculation a simplification is made, that is; the corners of the edge beams are assumed to be square. This results in a slightly too large calculated effective area.

Within the chosen effective area, there are six reinforcement bars, three with diameter 16 mm and three with diameter 20 mm. This gives a reinforcement area of:

$A_s = 3 \times \pi \times 8^2 + 3 \times \pi \times 10^2 = 1545.7\text{mm}^2$.

This gives:

$\rho_{p,eff} = 1545.7/133000 = 0.01$

The crack width is now calculated from Equation 3.43:

$w_k = \varepsilon_{cr}(3.4c + 0.425\frac{k_1 k_2 \phi}{\rho_{p,eff}}) = 0.22 \times 10^{-3} \times (3.4 \times 100 + 0.425 \times \frac{0.8\times16}{0.01})$

This gives $s_{r,max} = 408$ mm and $w_k = 0.19$ mm.

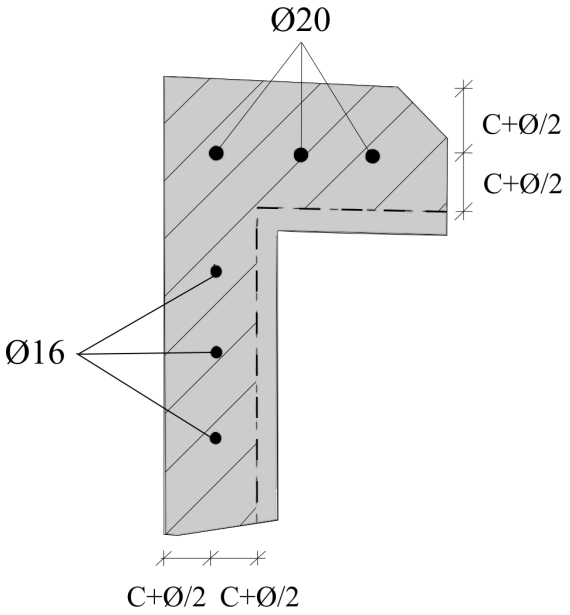

FIGURE 9.2: Simplified model for calculating the effective cross sectional area of the edge beams at Sandsgård Bridge.

Chapter 10

Calculation of Crack Widths in Structures with Combined Reinforcement

In this chapter, the theoretical crack widths of the different fiber concretes on the edge beams at Sandsgård Bridge are calculated. The calculations are performed according to the paper presented at Nordic Mini-seminar "Fiber reinforced concrete", *Calculation of crack width and crack spacing*, written by Ingemar Löfgren [2]. The method is presented in Section 3.1. The calculations of the laboratory experiment, that was done in conjunction with the specialization project, are also presented.

10.1 The Laboratory Experiment

In the specialization project written by the undersigned, a modified version of Löfgren's model was used to calculate the expected crack widths. In the laboratory experiment, the number of cracks was already known, and the model was used to calculate the theoretical crack widths. The average crack distance was set equal to the length of the member, and the number of cracks was hence set to 1. The reinforcement stress that fulfilled the compatibility requirement was used to calculate the crack width. The calculated widths were compared with the measured crack widths in the experiment. As mentioned in the introduction of this thesis, the measured crack widths were about double the size of the calculated crack widths. The results are repeated in Table 10.1.

TABLE 10.1: Average measured crack widths and maximum calculated crack widths for the edge beams in the laboratory experiment.

Concrete mix	Measured crack width (average)	Calculated crack width (maximum)
Reference mix	0.17	0.09
Concrete with steel fibers	0.03-0.04	0.02
Concrete with polymer fibers	0.06	0.03

10.2 Sandsgård Bridge

10.2.1 Procedure

In this procedure, the number of cracks, n, are increased until all the requirements are fulfilled. First, the reinforcement stress that fulfills the deformation requirement for $n = 1$, is found. Then, the force that acts on the uncracked parts, N, is calculated from the relevant reinforcement stress. If N is larger than the force needed to initiate a new crack, N_1, the number of cracks are increased by 1. The procedure is repeated until N_1 is larger than N. The calculations are performed in Excel, and the tool *Problem solver* is used to calculate the stresses.

10.2.2 Input Data

Based on experience, it is chosen to use the moduli of elasticity $E_s = 200000$ MPa and $E_c = 30000$ MPa for respectively the reinforcement and the concrete [15]. As in Section 9.2, it is also in this case assumed that the degree of restraint is equal to 1. The concrete shrinkage is set equal the sum of the temperature strain, the drying shrinkage and the autogenous shrinkage strain.

From Section 9.2, the drying shrinkage is calculated to $\varepsilon_{cd}(52) = 0.16$ ‰.

According to Eurocode 2, Part 1-1, 3.1.4 (6) [8] the autogenous shrinkage strain is given by the equation:

$$\varepsilon_{ca}(t) = \beta_{as}(t)\varepsilon_{ca}(\infty) = (1 - \mathrm{e}^{-0.2t^{0.5}}) \times 2.5(f_{ck} - 10) \times 10^{-6} \tag{10.1}$$

The deck was cast March 3, while the edge beams were cast 13 days later, March 17. When the crack mapping was performed, the age of the edge beams were 52 days and the age of the deck was 65 days. The autogenous shrinkage strain is calculated as the strain in the edge beams at an age of 52 days, minus the difference in autogenous shrinkage between the age of 65 and 13 days for the deck. This gives a strain difference of:

$$\Delta\varepsilon = \varepsilon_{ca}(52) - (\varepsilon_{ca}(65) - \varepsilon_{ca}(13)) = 0.042‰$$

The maximum temperature difference is modeled in Section 6.3, and equals 12.8 °C. Assuming that the thermal coefficient is 9×10^{-6}, this corresponds to a temperature strain of:

$\Delta\varepsilon_T = 12.8 \times 9 \times 10^{-6} = 0.12$ ‰

The total concrete shrinkage can now be calculated:

$\varepsilon_{cs} = 0.16$ ‰+0.042 ‰+0.12 ‰= 0.32 ‰

The effective concrete area is obtained from Section 9.2: $A_{ef} = 650 \times 146 + 254 \times 150 = 133000$ mm^2

The strength valid for concrete with characteristic compressive strength $f_{ck} = 45$ MPa is obtained from Eurocode 2, Table 3.1. The average compressive strength after 28 days is $f_{cm} = 53$ MPa. The tensile strength is $f_{ctm} = 3.8$ MPa.

Within the chosen effective area, there are six reinforcement bars, three with diameter 16 mm and three with diameter 20 mm. This gives a reinforcement area of:

$A_s = 3 \times \pi \times 8^2 + 3 \times \pi \times 10^2 = 1545.7\text{mm}^2$

The creep coefficient is obtained from Eurocode 2, Part 1-1, 3.1.4, Figure 3.1(b) [8]. From Section 9.2, h_0 is calculated to 70.1 mm. For $t_0 = 52$, normal class concrete and strength class C45/55 a creep coefficient of 1.5 is deduced.

The input data is listed in Table 10.2.

Table 10.2: Input data for the modified calculation model

E_s	200 000 MPa
E_c	30 000 MPa
R	1
ε_{cs}	0.32 ‰
f_{cm}	53 MPa
f_{ctm}	3.8 MPa
A_{ef}	133 000 mm^2
A_s	1545.7 mm^2

As calculated in Section 5.2, the listed values for the residual flexural tensile strength are used in the calculation:

- $f_{fres,steel} = 1.28\ N/mm^2$
- $f_{fres,polymer} = 0.28\ N/mm^2$
- $f_{fres,basalt} = 1.53\ N/mm^2$

10.2.3 Results

The results from the calculation performed in Excel, are listed in Table 10.4.

TABLE 10.3: The calculated maximum crack widths for the different fiber concretes at Sandsgård Bridge.

Fiber type	Number of cracks	Calculated crack width [mm]
Steel	4	0.26
Polymer	3	0.38
Basalt	5	0.22

10.3 Modification of the Model

In a modified version of the model, the number of cracks is already known, and the model is used to calculate the theoretical crack widths. During the field visit, it is likely to think that the crack pattern was not fully developed. Hence, the number of cracks, and consequently the average crack distance, are unknown, and an estimation of the crack distance is used. In this simplified case, the calculated maximum crack distance is assumed to be equal the average crack distance. The crack distance is set equal to the length of the member, and the number of cracks is hence set to 1. The reinforcement stress that fulfills the compatibility requirement is now used to calculate the crack width. The calculations are performed in Excel, and the tool *Problem solver* is used to calculate the stresses.

10.3.1 Input Data

The same input data that was used in Section 10.2.2 is also used for the simplified model. In addition, also the maximum crack distance is an input parameter. For fibre reinforced concrete, this value is calculated from *Draft Annex to EN 1992-1-1* [17], from the following equation:

$$l_{s,max} = k \times c + \frac{1}{4} \times \frac{f_{ct,eff}(1 - \alpha_{tF})}{\tau_{bm}} \times \frac{\phi_s}{\rho_{p,eff}} \tag{10.2}$$

where

- k is an empirical parameter to take the influence of the concrete cover into consideration. As a simplification $k = 1$ can be assumed [18]
- c is the concrete cover
- $f_{ct,eff}$ is the mean value of the tensile strength of the concrete effective at the time when the cracks may first be expected to occur: $f_{ct,eff} = f_ctm$ or lower, $(f_{ctm}(t))$, if cracking is expected earlier than 28 days [8]
- α_{tF} is the ratio f_{Ftsd}/f_{ctm}. f_{Ftsd} is the design value of the residual tesile strength for crack openings in the serviceability range, accounting for fibre orientation, volume and scale effects.
- $f_{Ftsd} = f_{Ftsk}/\gamma_{SF} = k_O k_G \alpha_{t1} f_{R1,k}/\gamma_{SF} = 1 \times 1 \times 0.4 \times 0.7 f_{R1,m}/1.5 \rightarrow f_{Ftsd} = 0.18 f_{R1,m}$

- τ_{bm} is equal to $1.8 f_{ctm}(t)$
- ϕ_s is the reinforcement bar diameter
- $\rho_{p,eff}$ is the ratio A_s/A_c

The crack mapping on Sandsgård Bridge was performed 52 days after casting of the edge beams. Therefore, the tensile strength of the concrete for $t = 52$ days is used. This equals 3.97 MPa, according to the calculation method presented in Eurocode 2, 3.1.2 (9) [8].

Inserting into Equation 10.2, the maximum crack distance is expressed by:

$l_{s,max} = 65 + \frac{1}{4} \times (3.8 \times (1 - 0.18 \times f_{R1,m}/3.8))/(1.8 \times 3.97) \times \frac{16}{0.01} = 65 + 212.7 \times (1 - 0.18 \times f_{R1,m}/3.8)$

$f_{R1,m}$ for each fiber concrete is obtained from Section 5.2. Finally, the maximum crack distance can be calculated.

Steel fiber concrete: $l_{s,max} = 65 + 212.7 \times (1 - 0.18 \times 2.85/3.8) = 249$mm

Polymer fiber concrete: $l_{s,max} = 65 + 212.7 \times (1 - 0.18 \times 0.62/3.8) = 271$ mm

Basalt fiber concrete: $l_{s,max} = 65 + 212.7 \times (1 - 0.18 \times 3.4/3.8) = 243$ mm

10.3.2 Results

The results from the calculations performed in Excel for the modified model, are listed in Table 10.4.

TABLE 10.4: The calculated maximum crack widths for the different fiber concretes at Sandsgård Bridge. The calculations are performed according to the modified calculation model.

Fiber type	Calculated crack width [mm]	$N_1 > N$
Steel	0.04	OK
Polymer	0.06	OK
Basalt	0.04	OK

Chapter 11

Discussion

The background for this thesis, is that cracks due to external restraint are observed on the edge beams of many of today's bridges. Hence, it was decided to perform a laboratory experiment, and afterwards a large scale experiment on a real bridge, on externaly restrainted edge beams. Three different models for calculating crack widths are used, and the stresses are also modeled in the finite element program CrackTeStCOIN.

11.1 Comparison of the Results

CrackTeStCOIN does not report strains, and it is therefore chosen to make a simplified calculation from an effective E-modulus. By assuming a creep coefficient of 2 for the laboratory experiment and 1.5 for Sandsgård Bridge, the strains are calculated on the same basis as the strains from the other calculation methods. The effective E-moduli may be calculated according to Eurocode 2, 7.4.3 (5):

$E_{eff}(\phi = 2) = (30000)(1 + 2) = 10000$ MPa

$E_{eff}(\phi = 1.5) = (30000)(1 + 1.5) = 12000$ MPa

Under this assumption the occurring stress during the hardening phase in the laboratory, corresponds to a tensile strain equal to:

$\varepsilon_{hardening} = 0.195/10000 = 0.02$ ‰.

During heating, the simulated maximum stress in the edge beam equals 5 MPa. This corresponds to a resulting maximum tensile strain of:

$\varepsilon_{heating} = 5/10000 = 0.5$ ‰

When using concrete *C40/50 Anlägg (Swe) w/c = 0.38 Air*, the simulated maximal occurring stress at Sandsgård Bridge equals 1.7 MPa. Under the assumption of an effective E-modulus of 12 000 MPa, this corresponds to a maximum tensile strain equal to 0.14 ‰. For concrete *Semi*

low-heat concrete, 20% FA, the maximum occurring stress equals 0.7 MPa, corresponding to a tensile strain of 0.06 ‰.

The resulting strains from CrackTeStCOIN and the different calculation methods are presented in Table 11.1. For simplicity, the different models are referred to as:

Shrinkage cracking in fully restrained members (ACI Structural Journal) - **Method 1**

Early-age thermal crack control in concrete (CIRIA C660) - **Method 2**

Structures with combined reinforcement (Ingemar Löfgren) - **Method 3**

TABLE 11.1: Comparison of the different calculated and simulated concrete strains for both the laboratory experiment and the large-scale experiment.

Calculation method	Concrete strain [‰] Laboratory experiment	Concrete strain [‰] Sandsgård Bridge
CrackTeStCOIN	0.50 (heating) 0.02 (hardening phase)	0.14/ 0.06
Method 1	0.48 (hardening and heating)	-
Method 2	0.18 (hardening phase)	0.22
Modified method 3	0.48 (hardening and heating)	0.32

As Table 11.1 illustrates, the different methods results in different strains, and it is difficult to state which of the methods that is the most appropriate. It is reasonable to assume that the modeling in CrackTeStCOIN is the most accurate estimate for the temperatures and stresses. This assumption is made on the basis that the program includes the real wind and temperature specifications for the ambient air, and that the correct dimensions are modeled. Hence is the degree of restraint more accurate than for the calculation models. Also, for the laboratory experiment, the shrinkage curves for the actual concrete is entered in the program. Strains, however, are not reported by the program, and has been estimated based on an effective E-modulus.

The concrete strain from Method 1 and Method 3 are calculated on the same basis, and are hence equal. The estimated strain from CrackTeStCOIN corresponds well with this value, and it is clear that for the given case, these three methods give strains in the same range. Hence, it is likely to believe that the actual occurring strain is somewhat in this range.

The strain calculated in Method 2 does not take into account the effect of the heating cables. Hence, this value is significantly lower, and not comparable with the values obtained from Method 1 and Method 3. For the hardening phase, Method 2 provides a considerably greater value than the simulated strain in CrackTeStCOIN. The simulated strain equals 0.02 ‰, while the strain calculated in Method 2 equals 0.18 ‰. This difference is likely because CrackTeStCOIN simulates the strain 50 hours after casting, while the calculation in Method 2 is performed 15 days after casting. Hence, it is reasonable that Method 2 gives a higher strain than CrackTeStCOIN.

Based on the strains, the expected crack widths are calculated. The measured and calculated crack widths for both experiments are presented in Table 11.2 and Table 11.3.

TABLE 11.2: Average measured crack widths and calculated crack widths for the edge beams in the laboratory experiment.

	Reference mix	Steel fiber	Polymer fiber
Measured (average)	0.17	0.04	0.06
Method 1 (maximum)	0.38	-	-
Method 2 (maximum)	0.073	-	-
Method 3 (maximum)	0.09	0.02	0.03

Table 11.2 shows that the measured and calculated crack widths for the laboratory experiment differ a lot. Under the assumption that the measured crack widths are correct, it is clear that none of the methods are sufficiently accurate for providing good estimates for crack widths for the given case. Further development of the methods is therefore necessary, so that they can describe the actual case better. It seems like Method 1 is conservative, while Method 2 and Method 3 provide too low estimates of the crack width. However, it is important to keep in mind that there exist some uncertainties in the measured crack widths. Firstly, the crack width should be measured in the same height as the reinforcement, but clearly, this was not possible to conduct. Also, the crack width is varying over the height of the beam, and the value depends on where the width is measured. Lastly, there are also some uncertainties in the accuracy of the measurements performed with the crack measuring microscope (binoculars).

Method 1 and Method 3 are designed for the case where the structure is restrained in both ends, and the distribution of the strain is uniform over the considered cross section (axial restraint). This is not the case for the edge beams in question. The edge beams are restrained along one edge (edge restraint). Method 2 is valid for edge restraint, and it is hence more likely that this method is more appropriate than the before mentioned.

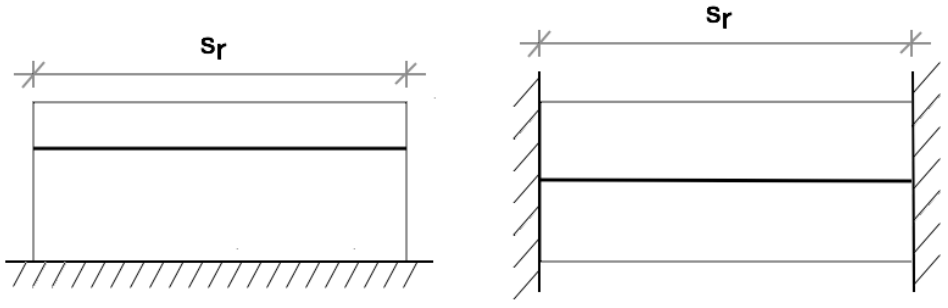

(a) Restraint along one edge, typical edge beam. (b) End restraint.

FIGURE 11.1: Edge and end restraint. In the figures, it is assumed that only one crack has occurred, and hence is the crack spacing set to the length of the member.

The presented crack widths in Table 11.3 differs a lot. The calculated crack width for the reference beam is approximately twice as big as the measured. This was not unexpected, as the crack widths are measured at an early age, and the crack pattern is hence not expected to be

Table 11.3: Average measured crack widths and calculated crack widths for the edge beams at Sandsgård Bridge.

	Reference mix	Steel fiber	Polymer fiber	Basalt fiber
Measured (average)	0.09	0.06	0.03	0.02
Method 2 (maximum)	0.19	-	-	-
Method 3 (maximum)	-	0.26	0.38	0.22
Modified Method 3 (maximum)	-	0.04	0.06	0.04

fully developed. The cracks are likely to widen over time, and it is therefore assumed that the measured values are too low.

The original and the modified version of Method 3 differ greatly from each other. It is hard to comment which method is the most accurate, but it is clear that both methods give an indication of the effect of the fiber reinforcement. For small crack widths, the steel fiber and basalt fiber provides approximately the same effect, while the polymer fiber restrains the cracks somewhat less (partly due to the low fiber amount). The measured crack width does not correspond well with the observed effect. This is likely because the crack mapping was performed before the crack pattern was stable. The measured values shows that the steel fiber concrete had wider crack widths than the other fiber concretes. This might be due to the fact that the steel fiber has a smooth surface, and hence may the fibers slide in its own track before it restraints the crack. It is assumed that the calculated effect shows better for larger crack widths.

11.2 Modeling in CrackTeStCOIN

There are many uncertainties in modeling in CrackTeStCOIN. There exist only a limited amount of materials to chose among in the program, and hence it is often necessary to chose a material with different properties than the one used in real life. For instance, the concrete used in the edge beams of Sandsgård Bridge is *CEM II/B-S 52.5 N (SV40)*, while the chosen concrete in CrackTeStCOIN is *C40/50 Anlägg (Swe) w/c = 0.38 Air*. This gives rise to differences between the modeled and the real values. However, it is possible to compare the logged temperatures from the edge beams with the simulated temperatures, to assess the validity of the simulation.

In the laboratory experiment the logged temperatures reached 70.4 °C right after the heating cables were turned off, while the simulated temperature in CrackTeStCOIN was 71.3 °C. This indicates that the simulated case corresponds well with the real case.

CrackTeStCOIN does not include the drying shrinkage in the modeling of the stresses, and hence it is reasonable to think that the real strain is slightly larger than the simulated strain. However, this will most likely not contribute to increase the stresses to a large extent. The considered cases are studied at an early age, when the drying shrinkage is low.

11.3 When do the Cracks Occur?

Cracks occur when the concrete stress reaches the tensile strength of the concrete. The tensile strength is time dependent, and hence must the occurring stress be compared with the tensile strength at the given time. The development of the tensile strength for a concrete in strength class C45/50, calculated from Eurocode 2, is shown in Figure 11.2. The crack mapping for the laboratory experiment was performed 369 hours after casting, which equals 15 days after casting. At this time, the tensile strength was 3.5 MPa. On Sandsgård Bridge, the crack mapping was performed 52 days after casting, corresponding to a tensile strength of 3.97 MPa.

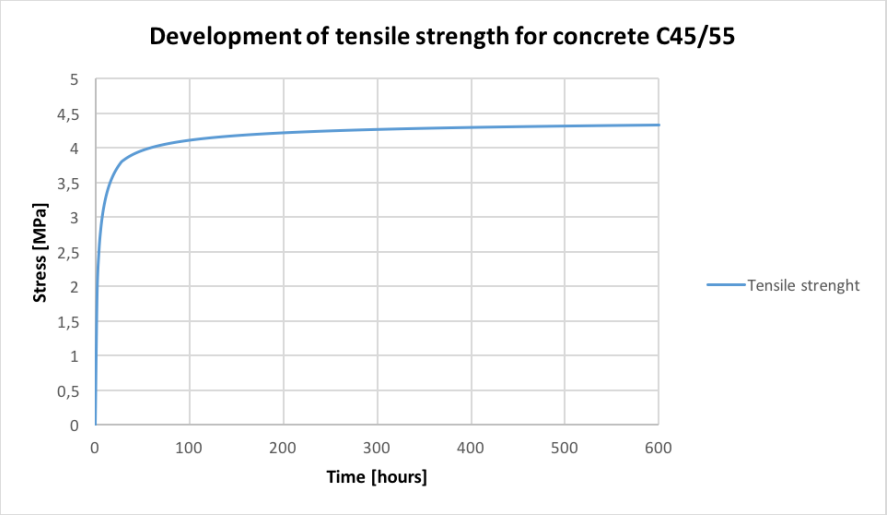

FIGURE 11.2: The development of tensile strength over time, for concrete in strength class C45/55.

Chapter 12

Concluding Remarks

In this thesis, the effect of fiber reinforcement on crack development was studied. A full-scale experiment on the bicycle and pedestrian bridge Sandsgård Bridge was performed, where the effect of steel, basalt and polymer fibers were assessed. A full crack mapping was conducted on the edge beams of the bridge, and the observed results were related to observations from a similar laboratory experiment performed earlier this year, which also are included in this thesis. Three different models for calculating the crack width are used. The most important results and conclusions from the work with this thesis are presented in the following.

Together with the laboratory experiment, the observations and calculations from this thesis show that fiber reinforcement has a favourable effect on the crack pattern in concrete structures. When adding fibers to the concrete mix, the hardened concrete will have a denser crack development with smaller crack widths than the reference concrete. Among the considered fiber types, steel fibers have been observed to have the greatest impact on the crack development. Secondly the basalt fibers, and lastly the polymer fibers. This effect, however, was not observed on Sandsgård Bridge. In this case the steel fiber concrete contained cracks with larger crack widths than the other fiber concretes. It is assumed that this is due to that the crack mapping was performed at an early stage, and hence was not the crack pattern fully developed.

In the laboratory experiment, the steel fibers reduced the average crack width by a factor of 4-5, while the polymer fibers reduced the crack width by a factor of 2-3. On the edge beams at Sandsgård Bridge the steel fibers reduced the crack width by a factor of 1.5, the polymer fibers by a factor of 3, and the basalt fibers reduced the average crack width by a factor of 4.5. The temperature history and correspindinig stresses were calculated with the computer program CrackTeStCOIN for both the laboratory experiment and the field test. The strains deduced from these calculations agree reasonably well with the calculated and the simplified methods. And the deviation can be explained. Therefore the largest uncertainty of the considered problem is due to the crack spacing.

A calculation method for combined reinforced concrete, developed by Ingemar Löfgren [2], was used to calculate the theoretical crack widths for all beams in both the lab experiment and the

field test. The calculated crack widths did not correspond well with the measured crack widths, but the model did, however, describe the positive effect of fiber in a qualitative way. Therefore, this model is promising and should be further developed. For structures with the same geometry and same amount of ordinary reinforcement, the calculation model gave reduced crack widths for the fiber concretes. Also, two other models for calculating crack widths in concrete with ordinary reinforcement are applied. The calculated crack widths differed significantly from the measured.

12.1 Further Work

Some suggestions for further work are listed as bullet points below:

- Assess which adjustments that can be made to adapting the presented calculation models to account for edge restraint.
- Follow up the crack development at Sandsgård Bridge, and compare the calculations with the measured crack widths from the stable crack pattern.
- Identify the crack spacing from other projects cast with ordinary reinforced concrete, and modify the formulas to account for fibres.

Bibliography

[1] Jacobsen, S et al. TKT 4215-Concrete Technology 1, 2009.

[2] Löfgren, I. Calculation of crack width and crack spacing. In *Nordic Mini Seminar: Fibre reinforced concrete, Trondheim, Norway*, pages 1–12, 2007.

[3] Kanstad, T and Kjellmark, G and Klausen, AEB. Forebygger sprekker i betongkonstruksjoner. *SINTEF Byggforsk Betonginnovasjon i Norge: Resultater fra forskningssenteret COIN (2007-2014)*, 2014.

[4] British Standards Institution. *Eurocode 2: Design of Concrete Structures: Part 3: Liquid retaining and containment structures*. British Standards Institution, 2006.

[5] Store norske leksikon. Kryp. URL https://snl.no/kryp.

[6] E Juliebø. Sentrale begreper og definisjoner innen betongfaget. URL http://www.iu.hio.no/bygglab/Betonglab/diverse/ordl_bet04.pdf.

[7] CJ Bernhardt. Krypning og svinn av betong ved forskjellige ytre forhold. *Nordisk Betong*, 1:9–26, 1967.

[8] British Standards Institution. *Eurocode 2: Design of Concrete Structures: Part 1-1: General Rules and Rules for Buildings*. British Standards Institution, 2004.

[9] Bamforth, PB. *Early-age thermal crack control in concrete*. Ciria, 2007.

[10] B Engström. Restraint cracking of reinforced concrete structures. *Division of Structural Engineering, Chalmers University of Technology, Göteborg*, 2008.

[11] IR Gilbert. Shrinkage cracking in fully restrained concrete members. *ACI Structural Journal*, 89(2):141–149, 1992.

[12] Pretec AS. Datablad - pieri curing clear.

[13] BS EN. 14651 (2007) test method for metallic fibre concretemeasuring the flexural tensile strength (limit of proportionality (lop), residual). *British Standard Institution, London*, 2005.

[14] Kanstad, T. Prvingsmetoder og evaluering av prveresultatene. *Utkast til Norsk betongforenings publikasjon nr 38*, 2014.

[15] Kjellmark, G and Klausen, A. Mechanical properties and calculation of model parameters for concrete with norcem cement and variable fly ash content. 2015.

[16] Bjntegaard, Ø and Kjellsen, K. Property development and cracking tendency in hardening concrete: Effect of cement type and fly ash content. *COIN Project report 40*, 2012.

[17] CEN/TC 250/SC 2/WG 1/TG 2 N 148. Draft annex to en 1992-1-1. 2015.

[18] Walraven, J et al. *Model Code 2010-First complete draft-Volume 2: Model Code*, volume 56. fib Fédération internationale du béton, 2010.

Appendix A

Drawings of Sandsgård Bridge

This appendix presents the calculation of the cross sectional area of the edge beam at Sandgsård Bridge, as well as some relevant drawings.

A.1 Reinforcement Drawing

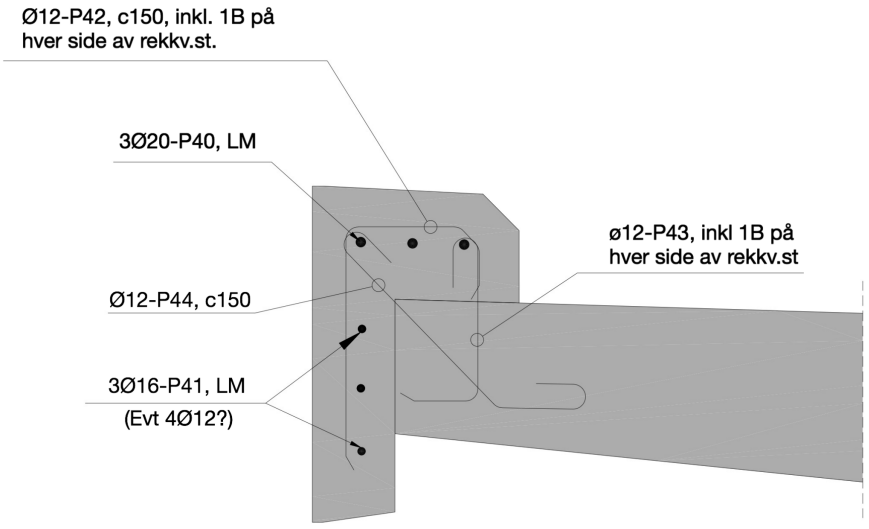

FIGURE A.1: The reinforcement drawing for the edge beams at Sandsgård Bridge.

A.2 Calculation of the Cross Sectional Area of the Edge Beams

To calculate the cross sectional area of the edge beams, the cross section is divided into 8 parts, illustrated in Figure A.2. The area for each part are calculated and summed up:

$A = 2\times(20\times20)/2+(20\times140)/2+610\times160+(20\times310)/2+170\times160+(70\times70)/2+140\times70 = 150450\ \text{mm}^2$

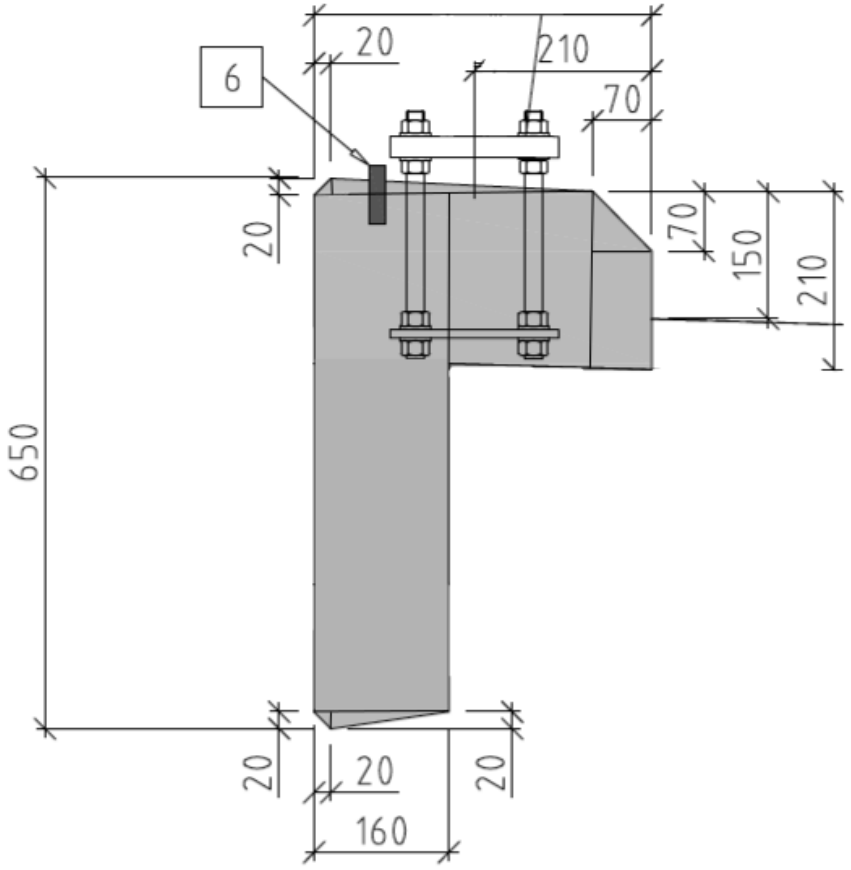

FIGURE A.2: Model for calculating the cross sectional area of the edge beams at Sandsgård Bridge.

A.3 Constructional drawings of Sandsgård Bridge

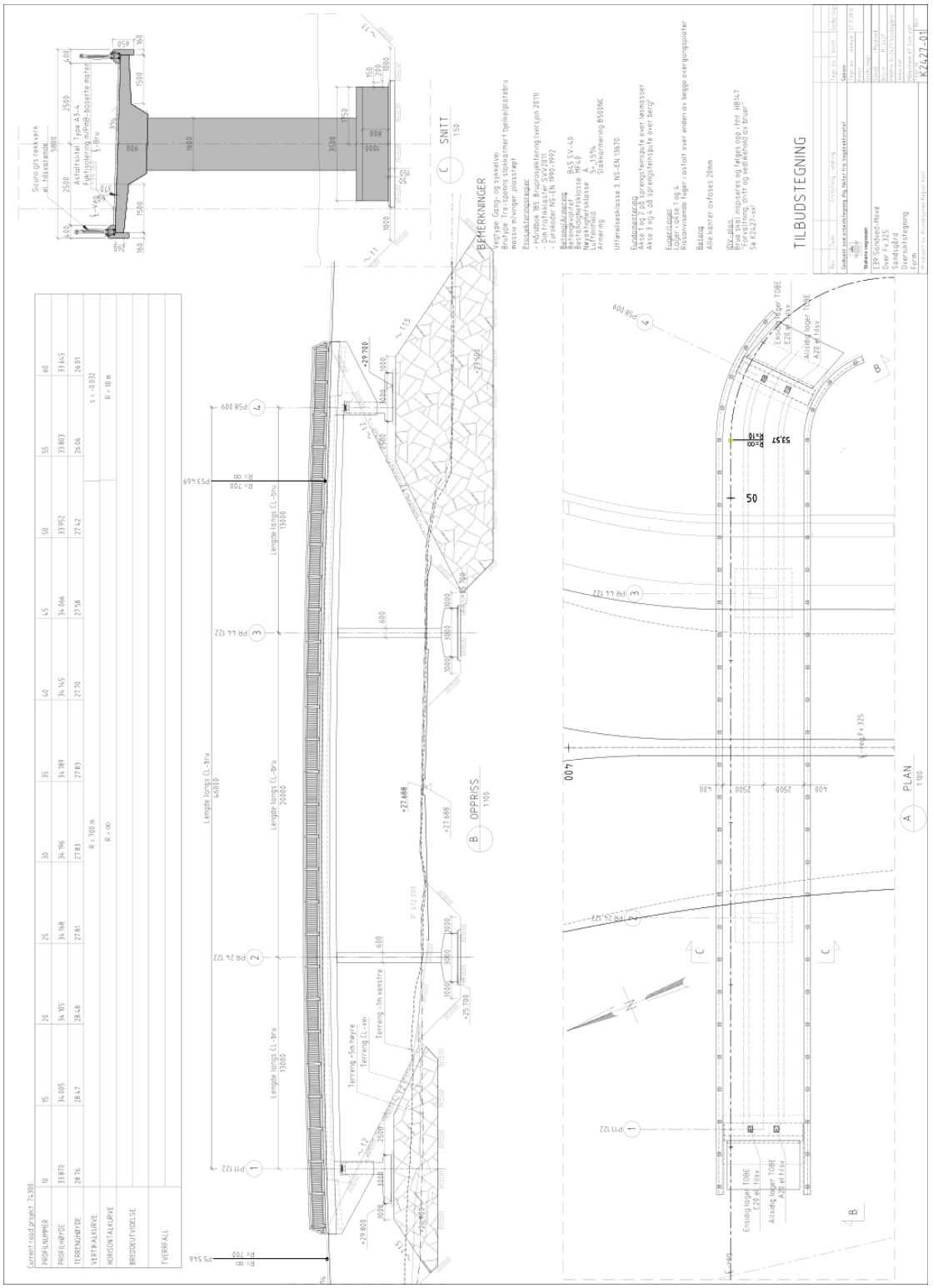

FIGURE A.3: General drawing of Sandsgård Bridge.

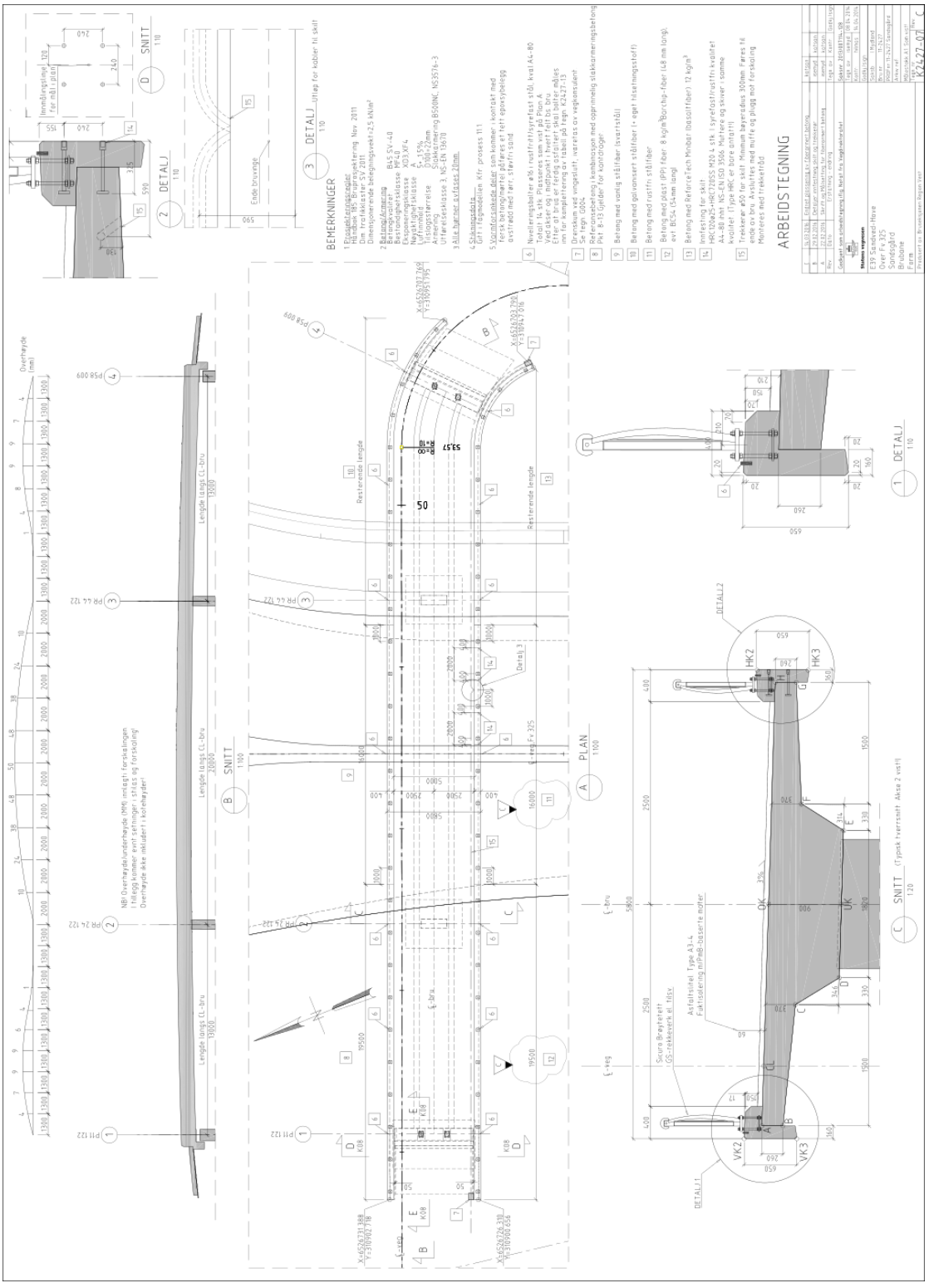

FIGURE A.4: General drawing of Sandsgård Bridge.

Appendix B

Residual Flexural Tensile Strength

This appendix presents the results from the calculations of the residual flexural tensile strength for the fiber concretes used at Sandsgård Bridge. The calculations are conducted by Researcher Giedrius Zirgulis at NTNU.

Load

Stainless steel	0,05	0,5	1,5	2,5	3,5	CMOD [mm]
	FLOP [kN]	FR1 [kN]	FR2 [kN]	FR3 [kN]	FR4 [kN]	
St1	15,0	8,3	9,1	10,2	9,2	
St2	16,0	7,7	9,5	10,5	8,6	
St3	15,3	7,2	7,6	9,5	0,5	
Average	**15,4**	**7,8**	**8,7**	**10,1**	**6,1**	

Plastic	0,05	0,5	1,5	2,5	3,5	CMOD [mm]
	FLOP [kN]	FR1 [kN]	FR2 [kN]	FR3 [kN]	FR4 [kN]	
P1	14,0	6,1	1,5	1,7	1,7	
P2	16,8	9,5	2,7	3,8	4,1	
P3	15,0	9,6	2,4	2,4	2,6	
Average	**15,3**	**8,4**	**2,2**	**2,6**	**2,8**	

Galvanised steel	0,05	0,5	1,5	2,5	3,5	CMOD [mm]
	FLOP [kN]	FR1 [kN]	FR2 [kN]	FR3 [kN]	FR4 [kN]	
G1	17,8	12,1	13,5	15,8	16,7	
G2	16,9	8,1	8,8	9,8	10,1	
G3	16,6	6,6	6,9	6,5	6,6	
Average	**17,1**	**8,9**	**9,7**	**10,7**	**11,1**	

Ordinary steel	0,05	0,5	1,5	2,5	3,5	CMOD [mm]
	FLOP [kN]	FR1 [kN]	FR2 [kN]	FR3 [kN]	FR4 [kN]	
O1	13,1	18,1	19,1	18,8	18,0	
O2	18,1	24,0	22,8	23,7	19,0	
O3	14,0	14,5	15,8	14,0	14,0	
Average	**15,1**	**18,9**	**19,2**	**18,8**	**17,0**	

Basaltic	0,05	0,5	1,5	2,5	3,5	CMOD [mm]
	FLOP [kN]	FR1 [kN]	FR2 [kN]	FR3 [kN]	FR4 [kN]	
B1	12,7	13,0	3,3	2,2	1,3	
B2	13,8	7,3	3,2	2,0	1,1	
B3	14,6	9,7	5,4	3,5	2,2	
Average	**13,7**	**10,0**	**3,9**	**2,6**	**1,5**	

Residaul flexural tensile strength

Stainless steel	0,05	0,5	1,5	2,5	3,5	CMOD [mm]
	fLOP [N/mm2]	fR1 [N/mm2]	fR2 [N/mm2]	fR3 [N/mm2]	fR4 [N/mm2]	
St1	5,1	2,8	3,1	3,4	3,1	
St2	5,5	2,7	3,3	3,6	3,0	
St3	5,2	2,5	2,6	3,3	0,2	
Average	**5,3**	**2,6**	**3,0**	**3,4**	**2,1**	

Plastic	0,05	0,5	1,5	2,5	3,5	CMOD [mm]
	fLOP [N/mm2]	fR1 [N/mm2]	fR2 [N/mm2]	fR3 [N/mm2]	fR4 [N/mm2]	
P1	4,8	2,1	0,5	0,6	0,6	
P2	5,7	3,3	0,9	1,3	1,4	
P3	5,2	3,3	0,8	0,8	0,9	
Average	**5,2**	**2,9**	**0,7**	**0,9**	**1,0**	

Galvanised steel	0,05	0,5	1,5	2,5	3,5	CMOD [mm]
	fLOP [N/mm2]	fR1 [N/mm2]	fR2 [N/mm2]	fR3 [N/mm2]	fR4 [N/mm2]	
G1	6,0	4,1	4,5	5,3	5,6	
G2	5,7	2,7	3,0	3,3	3,4	
G3	6,1	2,4	2,5	2,4	2,4	
Average	**5,9**	**3,1**	**3,4**	**3,7**	**3,8**	

Ordinary steel	0,05	0,5	1,5	2,5	3,5	CMOD [mm]
	fLOP [N/mm2]	fR1 [N/mm2]	fR2 [N/mm2]	fR3 [N/mm2]	fR4 [N/mm2]	
O1	4,5	6,1	6,5	6,4	6,1	
O2	6,1	8,1	7,7	8,1	6,4	
O3	4,8	4,9	5,4	4,8	4,8	
Average	**5,1**	**6,4**	**6,5**	**6,4**	**5,8**	

Basaltic	0,05	0,5	1,5	2,5	3,5	CMOD [mm]
	fLOP [N/mm2]	fR1 [N/mm2]	fR2 [N/mm2]	fR3 [N/mm2]	fR4 [N/mm2]	
B1	4,3	4,4	1,1	0,8	0,4	
B2	4,7	2,5	1,1	0,7	0,4	
B3	5,0	3,3	1,9	1,2	0,7	
Average	**4,7**	**3,4**	**1,3**	**0,9**	**0,5**	

FIGURE B.1: The measured loads from the test are presented in the table to the left. The calculated residual flexural tensile strengths are presented to the right.

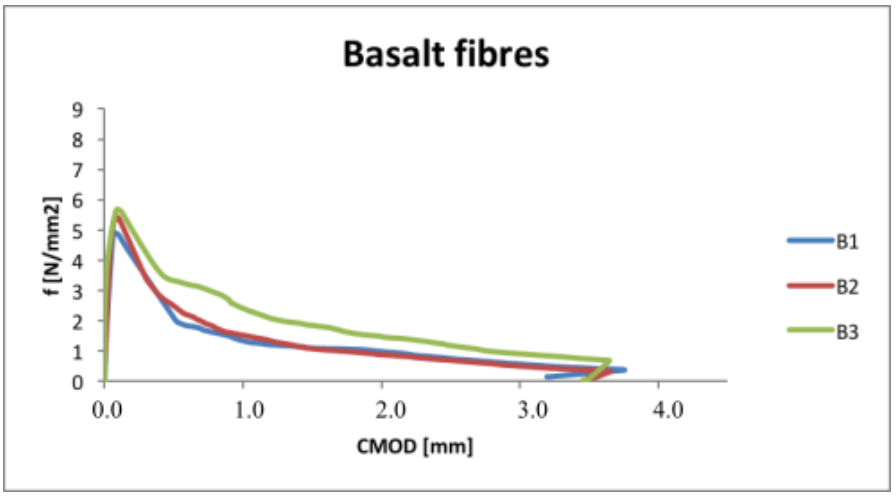

FIGURE B.2: The residual flexural tensile strength for the basalt fiber concrete, plotted as a function of the crack mouth opening displacement.

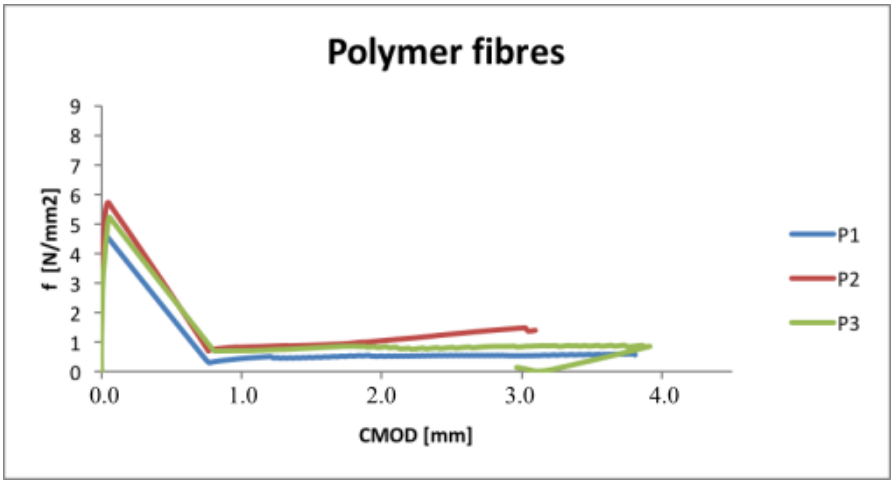

FIGURE B.3: The residual flexural tensile strength for the polymer fiber concrete, plotted as a function of the crack mouth opening displacement.

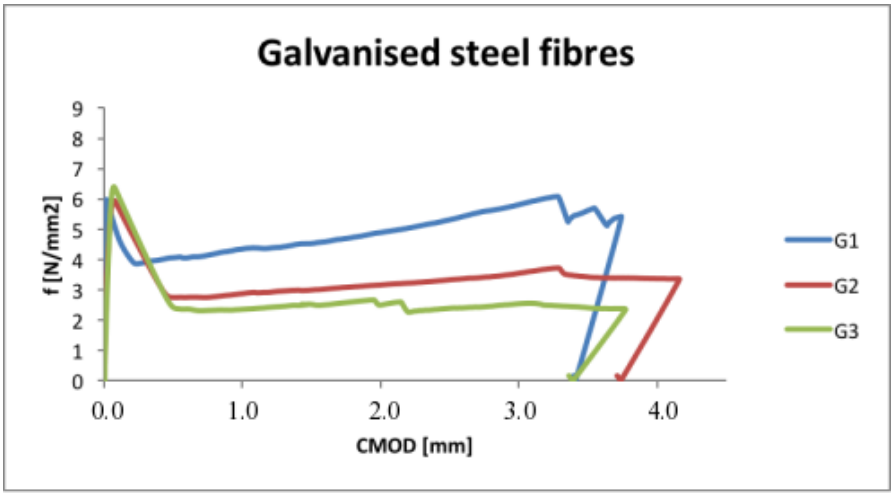

FIGURE B.4: The residual flexural tensile strength for the galvanized steel fiber concrete, plotted as a function of the crack mouth opening displacement.

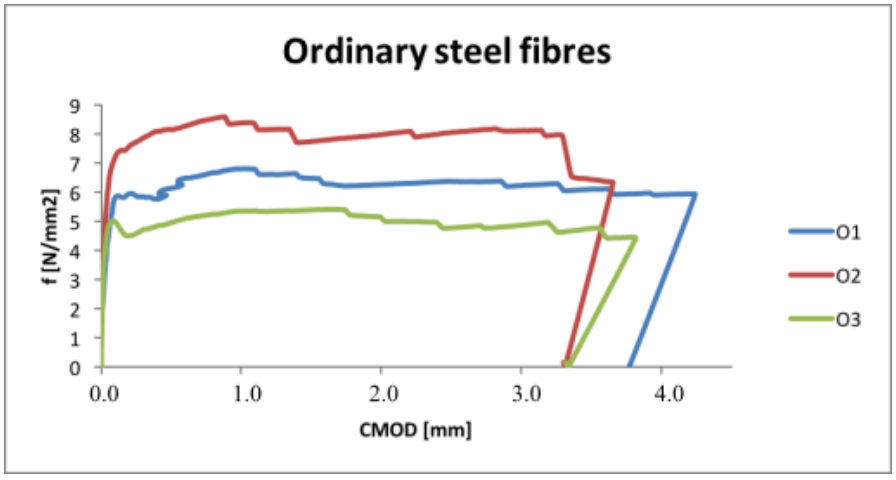

FIGURE B.5: The residual flexural tensile strength for the ordinary steel fiber concrete, plotted as a function of the crack mouth opening displacement.

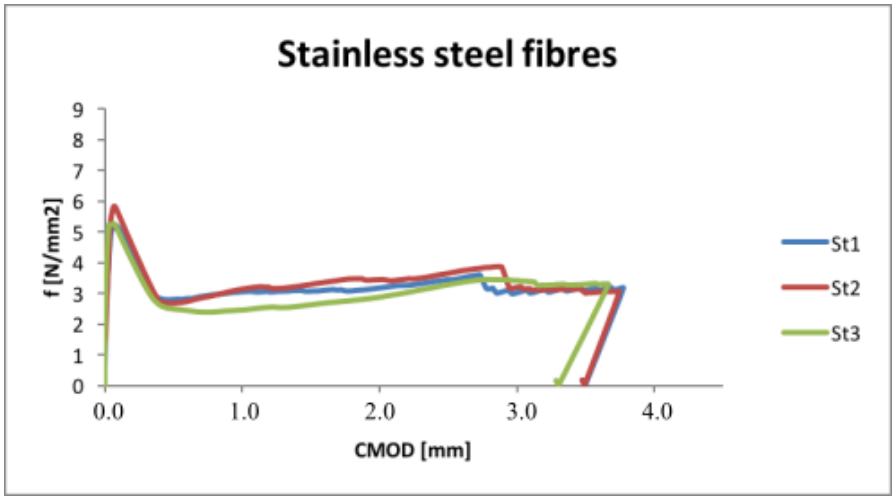

FIGURE B.6: The residual flexural tensile strength for the stainless steel fiber concrete, plotted as a function of the crack mouth opening displacement.

Appendix C

Temperature Development in Curing Boxes

The temperature development logged from the curing boxes for the reference concrete and the steel fiber concrete on Sandsgård Bridge is shown in Figure C.1 and Figure C.2.

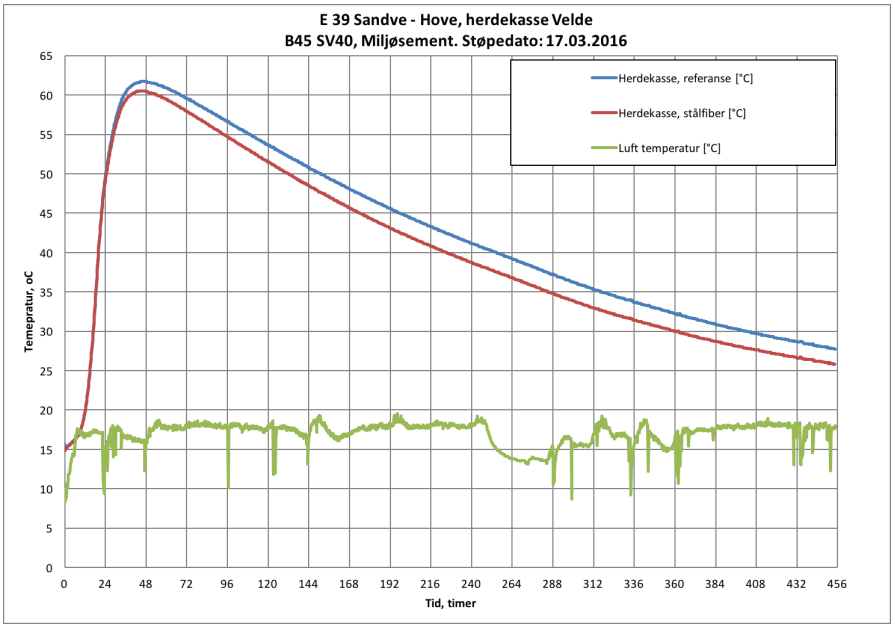

FIGURE C.1: Temperature development in the curing boxes during the first 456 hours after casting. The blue and red graphs show the temperatures in the reference beam and the steel fiber beam respectively, and the green graph shows the ambient temperature.

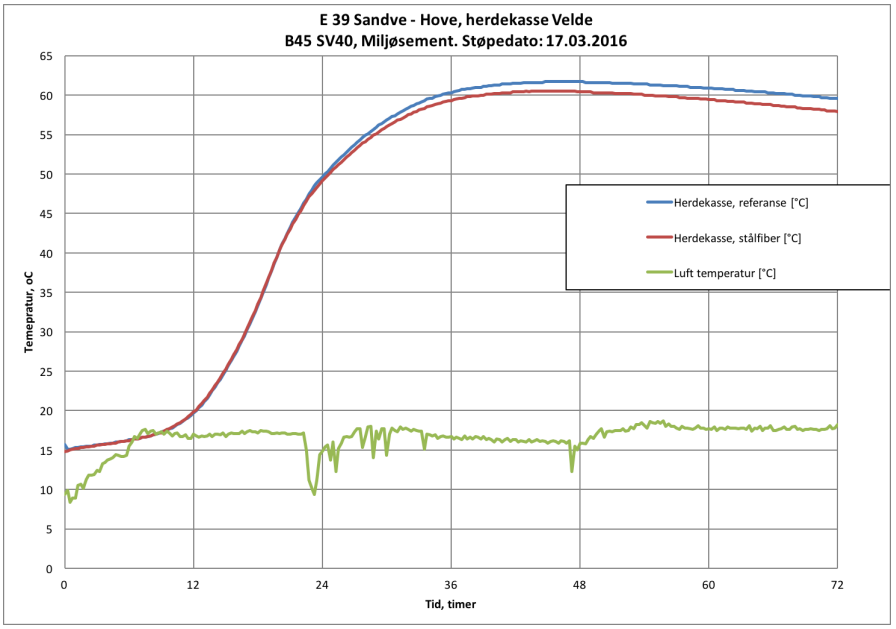

FIGURE C.2: Temperature development in the curing boxes during the first 72 hours after casting. The blue and red graphs show the temperatures in the reference and the steel fiber beam respectively, and the green graph shows the ambient temperature.